H. Xie, B. Wu, F. Bernelli Zazzera
High Minimum Inter-Execution Time Sigmoid Event-Triggered Control for Spacecraft Attitude Tracking with Actuator Saturation
IEEE Transactions on Automation Science and Engineering, Published online 15/06/2022
doi:10.1109/TASE.2022.3179896

High Minimum Inter-execution Time Sigmoid Event-triggered Control for Spacecraft Attitude Tracking with Actuator Saturation

Hongyi Xie, Baolin Wu, and Franco Bernelli-Zazzera

***Abstract*—This paper investigates the attitude tracking problem for spacecraft with limited communication, network congestion, unknown model parameters, actuator saturation, and external disturbances. To alleviate communication load, a novel sigmoid event-triggered mechanism is proposed with the special ability to guarantee a high minimum inter-execution time to avoid network congestion like package loss or time delay effectively. A neural network-based adaptive control algorithm is designed to deal with unknown model parameters. Besides, the problem of actuator saturation is tackled by introducing a dynamic loop gain function-based approach. System stability is proved by Lyapunov stability analysis and the high minimum inter-event time is substantiated by Zeno Behavior analysis with explanatory remarks. Numerical simulation results also show that a high minimum inter-event time and a high average inter-event time can be realized on the premise of high attitude tracking accuracy. Compared with all the previous studies, the ratio of the minimum inter-execution time to the average minimum inter-execution time has been improved by nearly 10 times with the proposed approach.**

***Note to Practitioners*—This paper was motivated by the problem of spacecraft attitude takeover control, but it also applies to other aperiodic discrete-time control systems. Existing event-triggered control methods have solved the problem of limited communication for attitude takeover control of spacecraft by reducing the number of times wireless communication is required. This paper proposes a new method for realizing quasi-periodic control with a large time gap between any two consistent control impulses using a hyperbolic tangent function or another sigmoid function in an event-triggered mechanism. The proposed sigmoid event-triggered mechanism (ETM) can magnify the event-triggered threshold dozens of times in a short time to avoid unnecessary frequent triggering without decreasing the precision of control. It's feasible to employ the proposed sigmoid ETM to deal with limited communication and network congestion in other network control systems that are constructed with similar dynamic structures. Furthermore, it would be marvelous if we could transform this sigmoid ETM into a high-efficiency decision-making mechanism in some control systems without using a wireless network. Now we are studying how to realize orbital-attitude (maneuver) control with a relatively average time interval and fewer times of orbit transfer by using the proposed sigmoid ETM.**

***Index Terms*—Attitude tracking, limited communication, network congestion, sigmoid event-triggered mechanism, actuator saturation.**

This work was supported by the National Natural Science Foundation of China under Grant 61873312, and the China Scholarship Council. Authors addresses: H. Xie and B. Wu are with the Research Center of Satellite Technology, Harbin Institute of Technology, Harbin 150001, China, E-mail: (10813726@polimi.it; wuba0001@e.ntu.edu.sg). H. Xie and F. Bernelli-Zazzera are with the Department of Aerospace Science and Technology, Politecnico di Milano, Milan 20156, Italy, E-mail: (hongyi.xie@polimi.it; franco.bernelli@polimi.it). (Corresponding author: Baolin Wu)

Manuscript received

I. Introduction

RECENTLY, the recycling of space debris and even the reuse of failed spacecraft are getting more and more attention. Up to February 2020, there were about 34,000 trackable objects in Earth's orbit, which put space activities in a risky situation. Nevertheless, even if the lifespan of a spacecraft ends because of depleted fuel or a fatal malfunction of any key subsystem, most high-valued devices fixed to a so-called "disabled spacecraft" would still work effectively [2], [3]. Now, with the invention of the cellular satellite [4], it's possible to extend the lifespan of some so-called "disabled spacecraft" or extract some high-valued payloads from disabled spacecraft by spacecraft takeover control [5]–[7] based on cellular satellites.

Cellular satellites are lots of standardized functional modules in correspondence to various subsystems of a monolithic spacecraft, and the abbreviation of a cellular satellite is "cell" [4]. Similar to the cells that make up different organs in one's body, several cellular satellites with typical functions can consolidate the subsystem of a spacecraft. Inversely, decomposing the subsystems of a spacecraft can give a series of cells. For example, the attitude control subsystem of a monolithic spacecraft can split into sensor cells, controller cells, and actuator cells. By contrast, all these cells can also make up the attitude control subsystem.

Motivated by cellular satellites, DARPA proposed the Phoenix program to dig up the residual value that remained in those disabled spacecraft [8]. Taking over the attitude control system of a disabled spacecraft to recover its proper functioning is a typical scene of the Phoenix program. In this circumstance, controller cells, sensor cells, and actuator cells will attach to different positions on the solar panels or the antenna of a disabled spacecraft to replace the disabled attitude control subsystems. Therefore, there are no communication wires between cells and disabled spacecraft, and also no wire connections among cells, so wireless communication is employed to transmit digital signals between different cells [7]. Consider that these cells are low-cost, small-sized functioning modules with limited wireless communication rates. It's necessary to consider the constraints of wireless network communication when designing the attitude takeover control system. Besides, it's necessary to deal with the problem of actuator saturation when designing the attitude takeover

control system. Restricted by the limited size of a cell, it's difficult for actuator cells to generate high torque outputs. Thus, the maximum value of control torques generated by the appropriate number of actuator cells is lower than those provided by large actuators.

Currently, several kinds of control algorithms have been developed to deal with the problem of spacecraft attitude tracking, including but not limited to adaptive control [9], [10], sliding-mode control [11], optimal control [12], model-predictive control [13], finite-time control [14], etc. Nevertheless, all these control schemes are periodic sampled control with control signals updated periodically. Hence, they cannot be employed to deal with limited communication directly.

In the field of control theory, there are two kinds of methods that have the ability to ease the communication load in a network control system: control with quantization [15], [16] and event-triggered control [17], [18]. In quantization control, a quantizer will convert continuous input signals to a finite number of quantization levels, and the signal transmission will occur if and only if the quantization level is changed [16], which implies the number of network trips will decrease a lot. Now the quantization method has been adopted to deal with limited communication in spacecraft attitude stabilization [19] and spacecraft attitude tracking [20], [21], which demonstrated the effectiveness of the quantization method in decreasing communication amounts by control system stability analysis and numerical simulation.

In event-triggered control, an event-triggered mechanism (ETM) based on the states of a network control system decides the switch of the sender units [17]. The transmission of signals only occurs when some system states (usually the system states error) violate the ETM at the triggering instants [18], which implies the signal transmissions only appear at the moments when they are needed. Now the ETM has also been employed to deal with limited communication in spacecraft attitude control [22]–[24]. On the premise of high precision attitude control, control stability analysis, Zeno behavior analysis, and numerical simulation show that the event-triggered method can decrease the amount of communication effectively.

However, although the previous studies [19] can reduce the amount of communication by a large margin to cope with the problem of limited communication, the risk of network congestion like time delay or package loss doesn't decrease after the employment of the quantization method or the event-triggered method, which is demonstrated by the equivalence of the MIET (minimum inter-execution time) and the corresponding step sizes of numerical simulation in [19]. In other words, all the previous studies can deal with the problem of limited communication in attitude control, but they cannot reduce the risk of network congestion, while the insurgence of the latter problem is more harmful and fatal for the network control system in many circumstances. Moreover, if the theoretical MIET is high enough, then it's possible to adopt a lower cost wireless network system with a lower frequency of communication in the network control system.

Now, in common spacecraft accurate attitude control systems, 8 Hz [25] are their normal frequency of signal transmission. If the network attitude control system proposed in [19] is applied, the amount of communication would be reduced a lot with enough precision of attitude control, while the MIET would still be 0.125s, which means it's still necessary to use the previous wireless network system with an 8 Hz frequency of communication to avoid any package loss or time delay. By contrast, if a high minimum inter-execution time network control system is invented with a 1 s minimum inter-execution time under the same requirement of control precision, then it's possible to adopt a 1 Hz wireless network system with a much lower cost in the attitude control system.

From the perspective of numerical simulation, in the field of spacecraft attitude control with limited communication, a model-based event-triggered control scheme [25] is effective in increasing the MIET without any explanation or analysis in theory. Besides, in [25], only the signal transmission between the sensor module and the controller module is aperiodic, while the signal transmission between the controller module and the actuator module is consecutive with a fixed step size of simulation, which seriously limits the application scope of this model-based method. To the best of the authors' knowledge, in the field of spacecraft attitude control, no method that can improve the MIET effectively with the corresponding theoretical basis has been proposed until now.

In the field of control theory, event-triggered control with a designable MIET is also a largely uncharted area, and a method that can improve the MIET several times is unheard of. In 2014, Antoine Girard established the lower bound of the MIET with the different event-triggered mechanisms that he proposed in [26]. He found that the so-called dynamic event-triggered mechanism is not clearly better than the common static event-triggered mechanism in improving the MIET. Nevertheless, Antoine still discussed and then gave out the interval location of the best MIET. The progress for higher MIET wasn't seen until 2019, when James Berneburg and Cameron Nowzari proposed a so-called "robust dynamic event-triggered" method with a designable minimum inter-execution time. Their paper, published in 2021 [27], was the first one to provide an event-triggered control scheme with a designable MIET. It's sure that the MIET can be improved by using their method, but the adjustable area of the MIET is quite limited. Because the aim of their method is to guarantee the existence of a definite lower bound of MIET that can be chosen by different agents in a distributed multi-agent system, the increase of MIET is not their main objective. Similarly, Shi et al. also gave a definite optimal theoretical lower bound for the MIET in [28]. However, there is a distance between knowing the exact optimal MIET or selecting the MIET for each agent in a multi-agent system and improving the MIET several times. The former two are concerning a problem of reliability with a certain positive-designable MIET that existed definitely. By contrast, the latter one is aimed at improving a concrete quality called MIET directly, which was not effectively solved by previous researchers, to the authors' best knowledge.

Furthermore, the thought of improving the MIET to decrease the probability of network congestion also opens a new door outside the TCP/IP model for network congestion avoidance, which is quite different from all the previous research in this domain. According to the authors' literature survey

about network congestion avoidance and control, the previous network congestion avoidance (control) approaches aimed to solve the problem within the TCP/IP model, especially on the layer of host to host. Typical network congestion avoidance and control schemes, such as TCP Tahoe, TCP Reno, and TCP Westwood+ [29], or the hybrid start approach of CUBIC [30], are designed to avoid network congestion by reducing the cwnd (congestion window) after detecting packet loss. The popular model-based approach called Bottleneck Bandwidth and Round-Trip Propagation Time (BBR) [31] may be close to the thought of the proposed method in this research since its core idea is to adjust the transmission rate, while the difference between BRR and the proposed high MIET event-triggered method is still obvious. The transmission rate of the network is directly adjusted by the BBR inside the TCP/IP model, while the high-frequency signals have been filtered by the high MIET ETM before they enter the wireless network. Recently, event-triggered control has also been employed in the field of network congestion control [29]. While similar to those slow start, hybrid start, or BBR network congestion control methods, the event-triggered congestion control method proposed in [32] still analyzes and solves the problem within the TCP/IP model. Besides, the minimum inter-execution time demonstrated in [32] is still equal to the step size of its numerical simulation. Thus, the quality of the event-triggered control system proposed in [32] can be greatly improved by introducing the sigmoid event-triggered mechanism with much higher inter-execution time.

Except for limited communication and network congestion, actuator saturation is also a core problem in spacecraft takeover control resulting from the narrow space supplied by a cell. However, actuator saturation is not considered in [19]–[25]. Jiang et al. in [33] developed an event-triggered control scheme for spacecraft attitude stabilization with actuator saturation. Nevertheless, attitude stabilization is only an exception to attitude tracking, with lower requirements for the design of the control system. Some other problems, such as fault-tolerant control [34] or the control allocation of actuators [35] for the mission of spacecraft attitude takeover control or attitude control with limited communication, have been studied by other researchers, so they are not the aims of this research.

Motivated by the mission requirements of spacecraft attitude takeover control, this paper proposes an adaptive event-triggered control scheme to tackle the problem of spacecraft attitude tracking with limited communication, unknown model parameters, actuator saturation, and external disturbances. In the designed control scheme, a sigmoid ETM is proposed to determine the triggering instants with a reasonable distribution. The control signals that the actuator received only changed at the triggering instants. Besides, to handle the unknown model parameters, an adaptive radial basis function neural network (RBFNN)-based term and another independent adaptive term are introduced to approximate the upper bound of the nonlinearity precisely, and then the virtual control torques without considering actuator saturation are generated. The virtual torques are tackled by a dynamic-loop gain function-based method to avoid input saturation, resulting in the actual control torques executed by the actuators. Moreover, the stability of the attitude tracking system is proved by the Lyapunov approach, and the high MIET effect of the sigmoid ETM with the corresponding criteria for selecting parameters is provided by Zeno behavior analysis. Finally, the validation of the proposed control scheme is illustrated by the numerical simulations.

Compared with all the existing attitude tracking schemes and all the existing network control systems, the main contribution of this paper is listed as follows:

1) The problem of spacecraft attitude tracking with limited communication is solved by the proposed sigmoid high MIET event-triggered control method. This method can reduce the amount of communication effectively and meet the requirement for tracking precision at the same time.

2) The problem of network congestion in the problem of spacecraft control with limited communication is discovered and solved in this paper. A simple sigmoid high MIET event-triggered control algorithm is proposed to increase the MIET by a large margin effectively, which means the requirement for communication frequency/costs of wireless network devices decreases a lot for the same mission as with a previous common event-triggered control system. Meanwhile, the proposed sigmoid event-triggered mechanism also opens a new direction of research outside of the TCP/IP model for network congestion avoidance.

3) The proposed dynamic loop gain function method can deal with input saturation, which is useful for dealing with the control problem of insufficient torque outputs.

The remainder of this work is laid out as follows. Problem formulation and related preliminaries are presented in section II. The design of the control law is given in section III, while the corresponding stability analysis and Zeno behavior analysis are given in section IV. Numerical simulation demonstrates the effectiveness of the proposed control scheme in section V. Finally, section VI concludes this research.

Notation: Both the inter-execution time and the inter-event time have the same meaning in this manuscript, which means the time length between two consistent triggerings. Furthermore, the average inter-execution time represents the mean value of all the values of inter-execution time observed, which also equals the ratio of the total time length to the times of triggering. Besides, the minimum inter-execution time denotes the shortest one picked from all the possible values of inter-execution time.

II. Problem Formulation and Preliminaries

A. Attitude tracking dynamics

It's reasonable to see the combination of a failed spacecraft and cellular satellites as a rigid spacecraft with the following dynamics model [9]:

$$\begin{aligned}\boldsymbol{J}\dot{\boldsymbol{\omega}}_e = &-\left(\boldsymbol{\omega}_e + \boldsymbol{C}\boldsymbol{\omega}_d\right)^{\times}\boldsymbol{J}\left(\boldsymbol{\omega}_e + \boldsymbol{C}\boldsymbol{\omega}_d\right)\\ &+\boldsymbol{J}\left(\boldsymbol{\omega}_e^{\times}\boldsymbol{C}\boldsymbol{\omega}_d - \boldsymbol{C}\dot{\boldsymbol{\omega}}_d\right) + \boldsymbol{u} + \boldsymbol{d}\end{aligned} \tag{1}$$

$$\dot{\boldsymbol{q}}_{v,e} = \frac{1}{2}\left(\boldsymbol{q}_{v,e}^{\times} + q_{0,e}\boldsymbol{I}_3\right)\boldsymbol{\omega}_e \tag{2}$$

$$\dot{q}_{0,e} = -\frac{1}{2}\boldsymbol{q}_{v,e}^{T}\boldsymbol{\omega}_e \tag{3}$$

TABLE I
NOMENCLATURE

Notations	Definitions
$\boldsymbol{\omega}(t)$	the body angular velocity of a spacecraft
$\boldsymbol{\omega}_e(t)$	the relative angular velocity errors
$\boldsymbol{\omega}_d(t)$	the expected angular velocity
$\boldsymbol{C}$	the rotation matrix
$\boldsymbol{J}$	the inertia matrix
$\boldsymbol{q}_{v,e}(t)$	the error quaternion vector
$q_{0,e}(t)$	the error quaternion scalar
J_{min}, J_{max}	the upper bound and the lower bound of $\boldsymbol{J}$
$\boldsymbol{d}(t)$	the external disturbances
$d_{\max}$	the upper bound of $\boldsymbol{d}(t)$
b_ω	the upper bound of $\boldsymbol{\omega}_d$
b_{ω_d}	the upper bound of $\|\dot{\boldsymbol{\omega}}_d\|$
$\boldsymbol{W}$	the desired neural network weight matrix
$\phi(\boldsymbol{X})$	the basis function vector
l	the number of the neural network codes
n	the serial number of a neural network code
μ_n	the receptive field center
H	the width of ϕ_n
W_M	the upper bound of $\boldsymbol{W}$
ϕ_M	the upper bound of ϕ
l_0	the Lipschitz constant
$\hat{\boldsymbol{W}}$	the estimated neural network weight matrix
$\widetilde{\boldsymbol{W}}$	the approximation error between $\hat{\boldsymbol{W}}$ and $\boldsymbol{W}$
$\delta_0(\boldsymbol{X})$	the estimation error of any nonlinear function $f(\boldsymbol{X})$
ε_0	the upper bound of $\|\delta_0(\boldsymbol{X})\|$
$\bar{u}_{max}$	the upper bound of the executed control torque
$\underline{u}_{min}$	the lower bound of the executed control torque
k_1	the sliding mode term parameter
k_2	the control gain
$\boldsymbol{s}$	the sliding mode vector
$\boldsymbol{L}$	the nonlinear term in attitude dynamics functions
L_1	the upper bound of one part of $\|\boldsymbol{L}\|$
L_2	the upper bound of the other part of $\|\boldsymbol{L}\|$
k	the serial number of the triggering instants
t_k	the documented moment of the k^{th} triggering instant
η	a design parameter about the estimation of L_1
σ, β, c	design parameters about the NN adaptive update
ρ	a design parameter about the estimation of L_2
$\hat{b}$	an estimated adaptive parameter about L_2
θ, θ_1	design parameters about the estimation of L_2
$\boldsymbol{\chi}$	the dynamic loop vector
φ	a constant about $\boldsymbol{\chi}$
$\boldsymbol{e}$	the event-triggered state errors
$\alpha, \gamma > 0$	design parameters in the ETM
β_1	the variable structure term in the ETM
c_1, μ_1	design parameters in β_1

where $\boldsymbol{\omega}_e(t) = \boldsymbol{\omega}(t) - \boldsymbol{C}\boldsymbol{\omega}_d(t)$. $\boldsymbol{\omega}(t) \in R^3$ represents the body angular velocity of the spacecraft relative to the inertial frame. $\boldsymbol{\omega}_d(t) \in R^3$ denotes the expected spacecraft attitude angular velocity relative to the inertial frame. $\boldsymbol{C}$ is the rotation matrix which describes the orientation of the body frame with respect to the desired frame. So $\boldsymbol{\omega}_e(t)$ denotes the relative angular velocity from the reference frame to the body frame, also represents the spacecraft's angular velocity error. Besides, the relative orientation from the reference frame to the body frame is described by the error quaternion, where $\boldsymbol{q}_{v,e}(t) \in R^3$ denotes the vector component of the error quaternion while $q_{0,e}(t) \in R$ is scalar component of the error quaternion, $\boldsymbol{q}_{v,e}(t) \in R^3$ and $q_{0,e}(t) \in R$ meet the identity ${\boldsymbol{q}_{v,e}}^T \boldsymbol{q}_{v,e} + {q_{0,e}}^2 = 1$. Furthermore, the disturbance torque is denoted by $\boldsymbol{d}(t) \in R^3$. $\boldsymbol{I}_3$ represents the 3×3 identity matrix, and the inertia matrix of the spacecraft is denoted by $\boldsymbol{J} \in R^{3\times 3}$. What's more, for a vector $\boldsymbol{a} = \begin{bmatrix} a_1 & a_2 & a_3 \end{bmatrix}^T$, the corresponding skew-symmetric matrix is defined as follows:

$$\boldsymbol{a}^\times = \begin{bmatrix} 0 & -a_3 & a_2 \\ a_3 & 0 & -a_1 \\ -a_2 & a_1 & 0 \end{bmatrix} \tag{4}$$

The following property and assumptions regarding spacecraft attitude dynamics are beneficial for the design of the controller and control stability analysis.

Property 1: The inertia matrix of the spacecraft $\boldsymbol{J}$ is symmetric and positive-definite. Moreover, it's restricted by the following inequation:

$$J_{\min}\|x\|^2 \le \boldsymbol{x}^T \boldsymbol{J} \boldsymbol{x} \le J_{\max}\|x\|^2, \forall \boldsymbol{J} \in R^3 \tag{5}$$

where J_{min} and J_{max} are constants regarding the size of the spacecraft.

Assumption 1 [19]: Wherever possible, the external disturbances $\boldsymbol{d}(t)$ are assumed to be upper bounded with $\|\boldsymbol{d}(t)\| \le d_{\max}$, where $d_{\max} > 0$.

Assumption 2 [19]: The desired spacecraft angular velocity $\boldsymbol{\omega}_d$ is upper bounded by $\|\boldsymbol{\omega}_d\| \le b_\omega$.Similarly, $\|\dot{\boldsymbol{\omega}}_d\| \le b_{\omega_d}$, where b_ω,$b_{\omega_d} > 0$.

B. Neural networks system

In the proposed control scheme, RBFNN is applied to estimate the nonlinear term with the unknown model parameter $\boldsymbol{J}$. The RBFNN can theoretically [36] approximate any continuous function over a compact set as follows:

$$f^*(\boldsymbol{X}) = \boldsymbol{W}^{*T}\phi(\boldsymbol{X}) + \delta^*(\boldsymbol{X}), \forall \boldsymbol{X} \in \Omega_x \tag{6}$$

where $\boldsymbol{W} \in \boldsymbol{R}^l$ denotes the desired constant NN weight matrix, $l > 1$ is the number of the neural network codes, $\delta^*(\boldsymbol{X})$ denotes the error of estimation with $|\delta^*(\boldsymbol{X})| \le \varepsilon^*$, $\varepsilon^* > 0$, $\varepsilon^* \to 0$. Besides, in this paper, $\phi(\boldsymbol{X}) = [\phi_1(\boldsymbol{X}), \phi_2(\boldsymbol{X}), \ldots, \phi_l(\boldsymbol{X})]^T$ is the basis function vector with the following Gaussian function based subfunction:

$$\phi_n(\boldsymbol{X}) = exp\left[-\frac{(\boldsymbol{X}+\mu_n)^T(\boldsymbol{X}-\mu_n)}{H^2}\right],\ n = 1, 2, \ldots,\ l \tag{7}$$

where μ_n is the receptive field center, H is the width of $\phi_n(\boldsymbol{X})$. There are two assumptions for the NN and the Gaussian function as follows:

Assumption 3 [37]: $\boldsymbol{W}$ is bounded on the upper side by $\|\boldsymbol{W}\| \le W_M$ and $\phi(\boldsymbol{X})$ is bounded on the upper side by $\|\phi(\boldsymbol{X})\| \le \phi_M$, where $W_M > 0, \phi_M > 0$ are unknown but existed.

Assumption 4 [37]: The Gaussian function $\phi(\boldsymbol{X})$ meets $\|\phi(\boldsymbol{X}_i) - \phi(\boldsymbol{X}_j)\| \le l_0\|\boldsymbol{X}_i - \boldsymbol{X}_j\|$, where $l_0 > 0$, is a known Lipschitz constant.

Furthermore, consider that $\boldsymbol{W} \in \boldsymbol{R}^l$ is unknown, it's sensible to define $\hat{\boldsymbol{W}}$ as the estimated NN weight matrix, which can be directly used by the controller. The approximation error is defined as $\widetilde{\boldsymbol{W}} = \boldsymbol{W} - \hat{\boldsymbol{W}}$. In the controller, a nonlinear function $f(\boldsymbol{X})$ can be approximated by

$$\hat{f}(\boldsymbol{X}) = \hat{\boldsymbol{W}}^T\phi(\boldsymbol{X}) \tag{8}$$

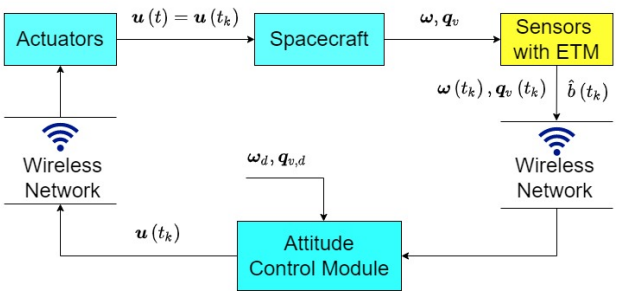

Fig. 1. Structure of the attitude tracking control scheme with sigmoid ETM

where $\hat{f}(\boldsymbol{X}) = f(\boldsymbol{X}) - \delta_0(\boldsymbol{X})$, $\delta_0(\boldsymbol{X})$ is the estimation error with the upper bound $|\delta_0(\boldsymbol{X})| \leq \varepsilon_0$, and $\varepsilon_0 > 0$ is a very small constant. $\hat{\boldsymbol{W}}$ follows $\|\hat{\boldsymbol{W}}\| \leq W_M$.

C. Problem Formulation

The aim of the research is to present an attitude tracking law with an event-triggered mechanism to reduce the amount of communication over the wireless communication channels and to avoid the risk of network congestion wherever possible. Besides, the proposed control scheme should have the ability to deal with actuator saturation and cater to the mission requirement of spacecraft attitude takeover control. Ultimately, the attitude tracking error and angular velocity tracking error must converge within a reasonable residual set in the presence of external disturbances.

Fig. 1 illustrates the structure of the proposed control scheme with ETM. The zero-order holds (ZOHs) in the ETM can store the latest states received at the last triggering-instant (also the moment that the latest wireless signal transmission occurs). If the differences between the ZOHs-held states and the sensor-measured states exceed the allowed range regulated by the ETM, the ETM is violated. Meanwhile, the wireless signal transmission via the sensor-controller channel or the controller-actuator channel will occur if and only if the ETM is violated. Therefore, the application of the ETM helps reduce unnecessary signal transmission in attitude tracking control, while the ETMs proposed in previous articles cannot avoid consecutive triggered events when system states vary violently. Thus, this paper aims to propose a kind of ETM that can improve the MIET a lot by suppressing the risk of network congestion like package loss or time delay as low as possible, instead of only easing the extent of limited communication as in previous research.

In practice, control signals that exceed the allowed range cannot be executed by an actuator. This situation of actuator saturation may influence the stability of the corresponding control system [38], and it's reasonable to give out the constraints of control torques as follows:

$$sat(u^*) = \begin{bmatrix} sat(u_1^*) & sat(u_2^*) & sat(u_3^*) \end{bmatrix}^T \tag{9}$$

where

$$sat(u_i^*) = \begin{cases} \bar{u}_{max} & u_i^* > \bar{u}_{max} \\ u_i^* & \underline{u}_{min} < u_i^* \leq \bar{u}_{max} \\ \underline{u}_{min} & u_i^* \leq \underline{u}_{min} \end{cases} \tag{10}$$

where $\bar{u}_{max} > 0$ and $\underline{u}_{min} < 0$ are the upper bound and the lower bound of the executed control torques, respectively. Commonly, $\bar{u}_{max} + \underline{u}_{min} = 0$. Besides, in this paper, the dynamic loop gain method is applied to deal with actuator saturation, and the following lemmas are employed in control stability analysis for the introduction of the dynamic loop gain method.

Lemma 1 [39]: If $\iota > 0, \zeta > 0, \widetilde{\rho}(t) > 0$, $\hat{\varpi}(t)$ follows $\dot{\hat{\varpi}}(t) = -\iota\hat{\varpi}(t) + \zeta\rho(t)$, then $\hat{\varpi}(0) > 0$ will result in $\hat{\varpi}(t) \geq 0$ as long as $t \geq 0$.

Lemma 2 [40](Barbalats Lemma): If a differentiable function $f(t)$ follows the following two conditions: (1) $\lim_{t\to\infty} f(t)$ is finite, $\dot{f}(t)$ is uniformly continuous. Then there exists $\lim_{t\to\infty} \dot{f}(t) = 0$.

Besides, the following lemma is useful here since the introduction of the hyperbolic tangent function in this paper:

Lemma 3 [24]: Given $\lambda > 0$, for any $x \in \mathbb{R}$, hyperbolic tangent function $tanh\left(\frac{x}{\lambda}\right)$ follows $0 \leq |x| - xtanh\left(\frac{x}{\lambda}\right) \leq \kappa\lambda$, where $\kappa = 0.2785$ meets $\kappa = exp(-\kappa - 1)$.

Lemma 4 [41]: Define smoothing functions $V(t_0, t) \geq 0$, $x(t) \geq 0$, $\varpi_g(t) \geq 0$ in $t \in [t_0, t_f)$. Define dynamic-loop gain function $N(x(t)) = e^{x^2(t)}x(t)$, bounded function $\bar{\tilde{s}}(t)$ and positive constant $\widetilde{s}$. If $V(t_0, t) \leq e^{-\tilde{s}t}\int_{t_0}^{t} \varpi_g N(x(\tau))\dot{x}(\tau)e^{\tilde{s}\tau}d\tau + e^{-\tilde{s}t}\int_{t_0}^{t} \dot{x}(\tau)e^{\tilde{s}\tau}d\tau + \bar{\tilde{s}}$ is true for any $t \in [t_0, t_f)$, then it's reasonable to deduce that $x(t)$, $V(t_0, t)$, $e^{-\tilde{s}t}\int_{t_0}^{t} \varpi_g N(x(\tau))\dot{x}(\tau)e^{\tilde{s}\tau}d\tau$ and $e^{-\tilde{s}t}\int_{t_0}^{t} \dot{x}(\tau)e^{\tilde{s}\tau}d\tau$ are bounded in $[t_0, t_f)$.

III. Sigmoid Event-Triggered Control Design

In this section, to realize attitude tracking control in the presence of limited communication, actuator saturation, unknown model parameters, and external disturbances, an adaptive controller is proposed with a sigmoid event-triggered mechanism to deal with limited communication and a dynamic-loop gain process to deal with actuator saturation. For designing the controller, it's reasonable to give out the definition of the sliding vector as follows:

$$\boldsymbol{s} = \boldsymbol{\omega}_e + k_1\boldsymbol{q}_{v,e} \tag{11}$$

where $k_1 > 0$. In the proposed event-triggered spacecraft attitude control scheme, $\boldsymbol{s}$ is consecutive varying on the sensor side. By contrast, the attitude control module receives discrete sliding mode vector signals $\boldsymbol{s}(t_k)$, since the wireless network only works at the triggering instants $t = t_k$, $k = 1, 2, \ldots$. At the triggering instant, the ETM is violated, and the control law is updated. Except for the triggering instants, the zero-order hold (ZOH) holds the constant sliding-mode vector received in the last triggering instant, and the error between the varying sliding mode vector and the held constant is defined as

$$\boldsymbol{e} = \boldsymbol{s} - \boldsymbol{s}(t_k), k = 1, 2, \ldots \tag{12}$$

Define the initial time of attitude tracking as $t_0 = 0$, then it's reasonable to find that $\boldsymbol{e} = 0$ at the triggering instants. Substituting (11) into (1) results in

$$\boldsymbol{J}\dot{\boldsymbol{s}} = \boldsymbol{L} + \boldsymbol{u} + \boldsymbol{d} \tag{13}$$

where $\boldsymbol{L}$ denotes the nonlinearity term in the dynamics model of spacecraft attitude tracking [25] as below:

$$\begin{aligned}\boldsymbol{L} = &-\left(\boldsymbol{\omega}_e + \boldsymbol{C}\boldsymbol{\omega}_d\right)^{\times}\boldsymbol{J}\left(\boldsymbol{\omega}_e + \boldsymbol{C}\boldsymbol{\omega}_d\right) + \boldsymbol{J}\boldsymbol{\omega}_e^{\times}\boldsymbol{C}\boldsymbol{\omega}_d \\ &- \boldsymbol{J}\boldsymbol{C}\dot{\boldsymbol{\omega}}_d + 0.5k_1\boldsymbol{J}\left(\boldsymbol{q}_{v,e}^{\times} + q_{0e}\boldsymbol{I}_3\right)\boldsymbol{\omega}_e\end{aligned} \tag{14}$$

For the common task of event-triggered attitude tracking without actuator saturation or unknown model parameters, it's sensible to develop a simple controller with high precision of attitude tracking as follows:

$$\boldsymbol{u}_{SPD} = -k_2\boldsymbol{s}\left(t_k\right) - \boldsymbol{L}\left(t_k\right) \tag{15}$$

Note that the inertial matrix $\boldsymbol{J}$ is an unknown model parameter that varies with the different attached positions of the cellular satellites, which follows $\|\boldsymbol{J}\| \le J_{max}$. Substituting $\|\boldsymbol{J}\| \le J_{max}$ into (14) leads to

$$\begin{aligned}\|\boldsymbol{L}\| &\le J_{max}\|\boldsymbol{\omega}\|^2 + J_{max}\left\|\boldsymbol{\omega}_e^{\times}\boldsymbol{C}\boldsymbol{\omega}_d\right\| \\ &+ J_{max}\left\|\dot{\boldsymbol{\omega}}_d\right\| + \frac{k_1}{2}J_{max}\|\boldsymbol{\omega} - \boldsymbol{C}\boldsymbol{\omega}_d\| \\ &\le J_{max}\left(\|\boldsymbol{\omega}\|^2 + \left\|\dot{\boldsymbol{\omega}}_d\right\| + \frac{k_1}{2}\|\boldsymbol{\omega}\| + \frac{k_1}{2}\|\boldsymbol{\omega}_d\|\right) \\ &+ J_{max}\left\|\frac{2\boldsymbol{\omega} - \boldsymbol{C}\boldsymbol{\omega}_d - \boldsymbol{C}\boldsymbol{\omega}_d}{2} \times \frac{2\boldsymbol{\omega} - \boldsymbol{C}\boldsymbol{\omega}_d + \boldsymbol{C}\boldsymbol{\omega}_d}{2}\right\| \\ &\le J_{max}\|\boldsymbol{\omega}\|^2 + J_{max}\left(\|\boldsymbol{\omega}_d\| + \frac{k_1}{2}\right)\|\boldsymbol{\omega}\| \\ &+ J_{max}\left(\frac{k_1}{2}\|\boldsymbol{\omega}_d\| + \left\|\dot{\boldsymbol{\omega}}_d\right\| + \frac{1}{2}\|\boldsymbol{\omega}_d\|^2\right)\end{aligned} \tag{16}$$

According to Assumption 2, it's reasonable to transform (16) into

$$\begin{aligned}\|\boldsymbol{L}\| \le J_{max}&\left[\|\boldsymbol{\omega}\|^2 + \left(b_\omega + \frac{k_1}{2}\right)\|\boldsymbol{\omega}\|\right] \\ &+ J_{max}\left(\frac{k_1}{2}b_\omega + b_{d\omega} + \frac{1}{2}b_\omega^2\right)\end{aligned} \tag{17}$$

For simplicity in control stability analysis, it's reasonable to define

$$\begin{cases} L_1 = J_{max}\left[\|\boldsymbol{\omega}\|^2 + \left(b_\omega + \frac{k_1}{2}\right)\|\boldsymbol{\omega}\|\right] \\ L_2 = J_{max}\left(\frac{k_1}{2}b_\omega + b_{d\omega} + \frac{1}{2}b_\omega^2\right)\end{cases} \tag{18}$$

Substituting (18) into (17) results in

$$\|\boldsymbol{L}\| \le L_1 + L_2 \tag{19}$$

Observed from (17), the upper limit of $\boldsymbol{L}$ is restricted by a polynomial regarding $\boldsymbol{\omega}$. To compensate $\boldsymbol{L}$ accurately for achieving high-precision estimation, it's feasible to approximate $L_1 = J_{max}\left[\|\boldsymbol{\omega}\|^2 + \left(b_\omega + \frac{k_1}{2}\right)\|\boldsymbol{\omega}\|\right]$ by an adaptive neural network approach. Meanwhile, approximate $L_2 = J_{max}\left(\frac{k_1}{2}b_\omega + b_{d\omega} + \frac{1}{2}b_\omega^2\right)$ by an easy adaptive compensation term. Thus, the structure of the controller without considering tackling actuator saturation can be proposed as follows:

$$\bar{\boldsymbol{u}} = \bar{\boldsymbol{u}}_a + \bar{\boldsymbol{u}}_b + \bar{\boldsymbol{u}}_c \tag{20}$$

where $\bar{\boldsymbol{u}}_a$ is a PD sub-controller designed as follows:

$$\bar{\boldsymbol{u}}_a = k_2\boldsymbol{s}\left(t_k\right), t_k \le t < t_{k+1} \tag{21}$$

where $k_2 > 0$. $\bar{\boldsymbol{u}}_b$ is proposed to approximate L_1,

$$\bar{\boldsymbol{u}}_b = \left|\hat{\boldsymbol{W}}^T\boldsymbol{\phi}\left(\|\boldsymbol{\omega}\left(t_k\right)\|\right)\right| Tanh\left[\eta\boldsymbol{s}\left(t_k\right)\hat{\boldsymbol{W}}^T\boldsymbol{\phi}\left(\|\boldsymbol{\omega}\|t_k\|\|\right)\right] \tag{22}$$

where $\eta > 0$ is a design parameter regarding J_{max} and $b_\omega + \frac{k_1}{2}$. $Tanh\left(\left[a_1\ a_2\ a_3\right]^T\right) = \left[tanh\left(a_1\right)\ tanh\left(a_2\right)\ tanh\left(a_3\right)\right]^T$. Besides, the adaptive update algorithm of $\hat{\boldsymbol{W}}$ is given as follows:

$$\begin{aligned}\hat{\boldsymbol{W}}^+ = &-\beta\frac{\left(\|\boldsymbol{\omega}\left(t\right)\| - \|\boldsymbol{\omega}\left(t_{k-1}\right)\|\right)\boldsymbol{\phi}\left(\|\boldsymbol{\omega}\left(t\right)\|\right)}{c + \left[\|\boldsymbol{\omega}\left(t\right)\| - \|\boldsymbol{\omega}\left(t_{k-1}\right)\|\right]^2} \\ &+ \left(1-\sigma\right)\hat{\boldsymbol{W}}, \qquad t = t_k, k = 1, 2, \ldots\end{aligned} \tag{23}$$

$$\dot{\hat{\boldsymbol{W}}} = 0, \quad t_k < t \le t_{k+1},\ k = 1, 2, \ldots \tag{24}$$

where $\sigma \in (0,1), \beta > 0, c > 0$ are design parameters.

Remark 1: In this paper, the neural networks only vary at the triggering instants. For simplicity in the stability analysis, it's reasonable to conceive that $\dot{\boldsymbol{W}} = \dot{\hat{\boldsymbol{W}}} = 0$, $t_k < t \le t_{k+1},\ k = 1, 2, \ldots$

To approximate $L_2 = J_{max}\left(\frac{k_1}{2}b_\omega + b_{d\omega} + \frac{1}{2}b_\omega^2\right)$, an additional but effective adaptive compensation term $\bar{\boldsymbol{u}}_c$ in the controller is proposed as follows:

$$\bar{\boldsymbol{u}}_c = \hat{b}Tanh\left[\rho\boldsymbol{s}\left(t_k\right)\right] \tag{25}$$

where $\rho > 0$ is a design parameter regarding $J_{max}\left(\frac{k_1}{2}b_\omega + b_{d\omega} + \frac{1}{2}b_\omega^2\right)$. Besides, $\hat{b}$ meets the following "augmented precision" adaptive law:

$$\dot{\hat{b}} = \theta\|\boldsymbol{s}\| - \theta_1\hat{b}, \hat{b}\left(0\right) \ge 0 \tag{26}$$

where $\theta > 0, \theta_1 > 0$, are design parameters. According to *Lemma 1*, there exists $\hat{b} > 0$ for any $t > 0$. Substituting (21)(22)(25) into (20) leads to

$$\begin{aligned}\bar{\boldsymbol{u}} = &k_2\boldsymbol{s}\left(t_k\right) + \hat{b}Tanh\left[\rho\boldsymbol{s}\left(t_k\right)\right] + \left|\hat{\boldsymbol{W}}^T\boldsymbol{\phi}\left(\|\boldsymbol{\omega}\left(t_k\right)\|\right)\right| \\ &\times Tanh\left[\eta\boldsymbol{s}\left(t_k\right)\hat{\boldsymbol{W}}^T\boldsymbol{\phi}\left(\|\boldsymbol{\omega}\left(t_k\right)\|\right)\right]\end{aligned} \tag{27}$$

Remark 2: Related numerical simulation verifies that, under the same simulation parameters, the steady-state errors resulting from a controller $\boldsymbol{u}_1 = -\bar{\boldsymbol{u}}$ are much smaller than the steady-state errors resulting from a similar controller $\boldsymbol{u}_2 = -k_2\boldsymbol{s}\left(t_k\right) - \left|\hat{\boldsymbol{W}}^T\boldsymbol{\phi}\left(\|\boldsymbol{s}\left(t_k\right)\|\right)\right| Tanh\left[\eta\boldsymbol{s}\left(t_k\right)\hat{\boldsymbol{W}}^T\boldsymbol{\phi}\left(\|\boldsymbol{s}\left(t_k\right)\|\right)\right]$, which shows the high precision of the controller designed as (27).

Although $\boldsymbol{u}_1 = -\bar{\boldsymbol{u}}$ can compensate for nonlinearity in attitude tracking efficiently, $\bar{\boldsymbol{u}}$ can be infinite with an infinite $\boldsymbol{s}$, which means $\boldsymbol{u}_1 = -\bar{\boldsymbol{u}}$ cannot cope with actuator saturation effectively. Hence, it's viable to adopt a dynamic loop gain method to process $\bar{\boldsymbol{u}}$ for dealing with actuator saturation. Based on the dynamic loop gain method, the actual control torques executed by the actuators are given as follows:

$$\boldsymbol{u} = -G\left(\boldsymbol{\chi}\right)^D\bar{\boldsymbol{u}} \tag{28}$$

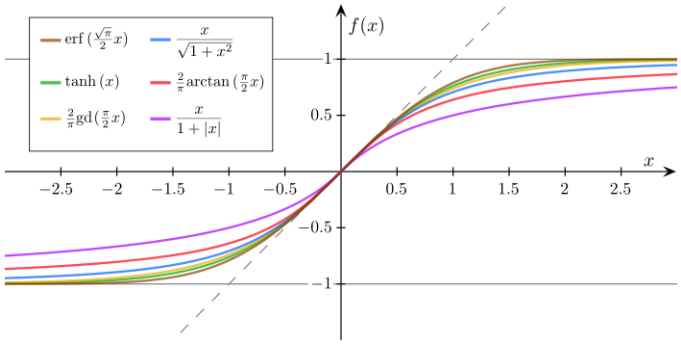

Fig. 2. Different kinds of Sigmoid Functiuons [42]

where $G(\boldsymbol{\chi})^D = diag[G(\chi_1) \quad G(\chi_2) \quad G(\chi_3)]$, $\boldsymbol{\chi} = [\chi_1 \quad \chi_2 \quad \chi_3]^T$, and $\boldsymbol{\chi}$ follows:

$$\dot{\boldsymbol{\chi}} = \varphi \boldsymbol{s}^D \bar{\boldsymbol{u}} \tag{29}$$

where $\varphi > 0$, $\boldsymbol{s}^D = diag[s_1 \ s_2 \ s_3]$. Besides, the dynamic loop function $\boldsymbol{\chi}$ follows:

$$G(\chi_i(t)) = e^{\chi_i^2(t)}\chi_i(t), \quad i = 1,2,3 \tag{30}$$

Combining (28)-(30) yields

$$\begin{aligned} u_i &= -\frac{1}{\varphi s_i}G(\chi_i)\frac{d\chi_i}{dt} = -\frac{1}{2\varphi s_i}2\chi_i e^{\chi_i^2(t)}\frac{d\chi_i}{dt} \\ &= -\frac{1}{2\varphi s_i}e^{\chi_i^2(t)}\frac{d\chi_i^2(t)}{dt} = -\frac{1}{2\varphi s_i}\frac{de^{\chi_i^2(t)}}{dt} \end{aligned} \tag{31}$$

Substituting (27) into (29) leads to

$$\begin{aligned} \frac{d\chi_i}{dt} &= \varphi s_i(t)\, s_i(t_k) + \hat{b}\varphi s_i(t)\, tanh[\rho s_i(t_k)] + s_i(t) \\ &\cdot\varphi\left|\hat{\boldsymbol{W}}^T\boldsymbol{\phi}\left|\left|\left|\boldsymbol{\omega}(t_k)\right|\right|\right|\right| tanh\left[\eta s_i(t_k)\,\hat{\boldsymbol{W}}^T\boldsymbol{\phi}\left|\left|\left|\boldsymbol{\omega}(t_k)\right|\right|\right|\right] \end{aligned} \tag{32}$$

According to (31), $\boldsymbol{u}$ is upper bounded as long as χ_i is upper bounded. From (32), χ_i is upper bounded as long as $s_i(t)$, and $\hat{b}$ are upper bounded. Considering that the boundedness of $s_i(t)$ and $\hat{b}$ is achieved by control stability analysis, it's reasonable to say the dynamic-loop control gain method is capable of restricting the size of $\boldsymbol{u}$ to avoid actuator saturation. For a controller which meets (23)(24), and (26-29), it's reasonable to realize high-reliability attitude takeover control by proposing the sigmoid event-triggered mechanism (SETM) as follows:

$$t_{k+1} = min\{t \geq t_k : \|\boldsymbol{e}\| \geq \beta_1(\alpha\|\boldsymbol{s}\| + \gamma)\} \tag{33}$$

where $k = 0,1,2,\ldots$, and $\alpha, \gamma > 0$ are design parameters. Furthermore, the variable structure term β_1 follows:

$$\beta_1 = 1 + c_1 - c_1 tanh\left(\frac{\mu_1}{k_1\left\|\boldsymbol{q}_{v,e}\right\| + \|\boldsymbol{\omega}_e\|}\right) \tag{34}$$

where $c_1, \mu_1 > 0$ are design parameters, and the following remark explains how to select appropriate parameters in (33-34).

Remark 3: According to the MIET analysis, any sigmoid function in Fig. 2 can be used to replace the hyperbolic tangent function in $\beta_1 = 1 + c_1 - c_1 tanh\left(\frac{\mu_1}{k_1\|\boldsymbol{q}_{v,e}\| + \|\boldsymbol{\omega}_e\|}\right)$. Because a dutiful β_1 only needs to satisfy the following two conditions:
(1) β_1 is expected to be large enough when $\|\boldsymbol{s}\| \to 0$
(2) β_1 is expected to be about 1 when $\|\boldsymbol{s}\|$ is very high

IV. Stability Analysis and Zeno Behavior Analysis

In this section, the stability of the proposed closed-loop high MIET event-triggered control system is analyzed based on an impulsive system approach [37]. According to [37], it's reasonable to analyze the system stability by classification. Define the dynamics during the flowing period $t_k \leq t < t_{k+1}$, as flowing dynamics, and define the dynamics at the triggering instants (jumping instants) $t = t_k, \ k = 1,2,\ldots$ as jumping dynamics, then it's rational to carry out the stability analysis for these two different situations separately.

Besides, Zeno behavior analysis based on control stability analysis can prove the effectiveness of the event-triggered mechanism without the existence of Zeno behavior. The Zeno behavior analysis is also used to compute the shortest inter-execution time and to reveal the inner logic of high MIET.

A. Stability analysis of the neural networks

The first step of stability analysis is to verify the ultimate boundedness of the proposed neural network by the following theorem.

Theorem 1: According to Assumption 3 and Assumption 4, $\|\tilde{\boldsymbol{W}}\| = \left\|\boldsymbol{W} - \hat{\boldsymbol{W}}\right\|$ is uniformly ultimately bounded with the application of the controller (27) which follows the adaptive updated laws (23-24).

Proof: Choose the following Lyapunov candidate function for $\tilde{\boldsymbol{W}}$:

$$V_{\tilde{W}} = \tilde{\boldsymbol{W}}^T(t)\,\tilde{\boldsymbol{W}}(t) \tag{35}$$

Then it's reasonable to demonstrate the ultimate boundedness of $\|\tilde{\boldsymbol{W}}\|$ by the integrated flowing dynamics analysis and jumping dynamics analysis as follows:

Case 1 (Flowing dynamics, $t_k < t \leq t_{k+1}, \ k = 1,2,\ldots$):

Derivate (35) by time t leads to

$$\dot{V}_{\tilde{W}} = \dot{\tilde{\boldsymbol{W}}}(t)\,\tilde{\boldsymbol{W}}(t) = 0 \tag{36}$$

(36) demonstrates that the ultimate boundedness of $\|\tilde{\boldsymbol{W}}\|$ is not up to flowing dynamics, and it's honest to claim that $\|\tilde{\boldsymbol{W}}\|$ is ultimately bounded as long as the ultimate boundedness of $\|\tilde{\boldsymbol{W}}\|$ is proved at the triggering instants.

Case 2 (Jumping dynamics, $t = t_k, \ k = 1,2,\ldots$):

(35) is discrete at the triggering instants, and the first derivative of (35) is

$$\boldsymbol{\Delta}V_{\tilde{W}} = \tilde{\boldsymbol{W}}^{T+}\tilde{\boldsymbol{W}}^{+} - \tilde{\boldsymbol{W}}^T\tilde{\boldsymbol{W}} \tag{37}$$

Consider $\hat{\boldsymbol{W}} = \boldsymbol{W} - \tilde{\boldsymbol{W}}$, then substitute (23) into (37) to get

$$\begin{aligned} \Delta V_{\tilde{W}} \leq &\left[\left(1 + \sigma + \sqrt{1+4\sigma}\right)\|\tilde{\boldsymbol{W}}\| + \beta_1\phi_M + \sigma W_M\right] \\ &\times\left[\left(1 + \sigma - \sqrt{1+4\sigma}\right)\|\tilde{\boldsymbol{W}}\| + \beta_1\phi_M + \sigma W_M\right] \end{aligned} \tag{38}$$

Note that $\left(1+\sigma+\sqrt{1+4\sigma}\right)\|\widetilde{\boldsymbol{W}}\|+\beta_1\phi_M+\sigma W_M \geq 0$. Thus, $\boldsymbol{\Delta}V_{\widetilde{W}} \leq 0$ is true when

$$\left(1+\sigma-\sqrt{1+4\sigma}\right)\|\widetilde{\boldsymbol{W}}\|+\beta_1\phi_M+\sigma W_M \leq 0 \tag{39}$$

Consider that $\beta_1\phi_M+\sigma W_M \geq 0$, $1+\sigma-\sqrt{1+4\sigma} \geq 0$, and $\|\widetilde{\boldsymbol{W}}\|$ will decrease if $\|\widetilde{\boldsymbol{W}}\|$ satisfies

$$\|\widetilde{\boldsymbol{W}}\| \geq \left(\beta_1\phi_M+\sigma W_M\right)/\left(\sqrt{1+4\sigma}-1-\sigma\right) \tag{40}$$

Therefore, $\|\widetilde{\boldsymbol{W}}\|$ is uniformly ultimately bounded. ■

B. Stability analysis of the proposed control system

On the basis of *Theorem 1*, it's reasonable to analyze the system stability by proving the following theorem:

Theorem 2: Consider the attitude tracking model of spacecraft (1-3), lemmas 1-4, the inequation (17), the adaptive update algorithms of NN (23) and (24), the "augmented precision" adaptive law (26), the dynamic-loop gain adaptive law (29), the high MIET sigmoid event-triggered mechanism (33) and (34), and the ultimate bound of NN $\|\widetilde{\boldsymbol{W}}\| \leq \left(\beta_1\phi_M+\sigma W_M\right)/\left(\sqrt{1+4\sigma}-1-\sigma\right)$. If Assumptions 1-4 hold and the control law (27) is implemented, then all the signals of the proposed control system, including $\left\|\boldsymbol{q}_{v,e}\right\|$, $\|\boldsymbol{\omega}_e\|$ are ultimately uniformly bounded, which means $\left\|\boldsymbol{q}_{v,e}\right\|$, $\|\boldsymbol{\omega}_e\|$ will converge within a small set.

Proof: The following proof is separated into two different parts, including flowing dynamics analysis and jumping dynamics analysis.

Case 1 (Flowing dynamics, $t_k < t \leq t_{k+1},\ k=1,2,\ldots$):

During the flowing period, consider the following Lyapunov function candidate:

$$V_f = \widetilde{\boldsymbol{W}}^{\,T}(t)\,\widetilde{\boldsymbol{W}}(t)+\frac{1}{2}\boldsymbol{s}^T\boldsymbol{J}\boldsymbol{s}+\frac{1}{2\theta}\widetilde{b}^2 \tag{41}$$

From (13)(26)(36), the time derivative of (41) is

$$\begin{aligned}\dot{V}_f &= \boldsymbol{s}^T\boldsymbol{J}\dot{\boldsymbol{s}}-\frac{1}{\theta}\widetilde{b}^T\dot{\hat{b}} = \boldsymbol{s}^T\left(\boldsymbol{L}+\boldsymbol{u}+\boldsymbol{d}\right)-\frac{1}{\theta}\widetilde{b}\left(\theta\|\boldsymbol{s}\|-\theta_1\hat{b}\right)\\ &= \boldsymbol{s}^T\left(\boldsymbol{L}+\boldsymbol{u}+\boldsymbol{d}\right)-\frac{1}{\theta}\widetilde{b}\left(\theta\|\boldsymbol{s}\|-\theta_1\hat{b}\right)\end{aligned} \tag{42}$$

Substituting (19)(20)(28) into (42) leads to

$$\begin{aligned}\dot{V}_f \leq\ & d_{max}\|\boldsymbol{s}\|-\boldsymbol{s}^T G(\boldsymbol{\chi})^D\bar{\boldsymbol{u}}_a+\left[L_1\|\boldsymbol{s}\|-\boldsymbol{s}^T G(\boldsymbol{\chi})^D\bar{\boldsymbol{u}}_b\right]\\ &+\left[L_2\|\boldsymbol{s}\|-\boldsymbol{s}^T G(\boldsymbol{\chi})^D\bar{\boldsymbol{u}}_c\right]+\left(\frac{\theta_1}{\theta}\widetilde{b}\hat{b}-\widetilde{b}\|\boldsymbol{s}\|\right)\end{aligned} \tag{43}$$

Apply *Lemma 3* to $\left(\frac{\theta_1}{\theta}\widetilde{b}\hat{b}-\widetilde{b}\|\boldsymbol{s}\|\right)$ in (43) to acquire the following inequation

$$\begin{aligned}&\frac{\theta_1}{\theta}\widetilde{b}\hat{b}-\widetilde{b}\|\boldsymbol{s}\| \leq \frac{\theta_1}{\theta}\left(b^2-\widetilde{b}^2\right)-\widetilde{b}\|\boldsymbol{s}\|-\hat{b}\|\boldsymbol{s}(t_k)\|\\ &+\hat{b}\|\boldsymbol{s}(t_k)\|+\boldsymbol{s}(t_k)^T\bar{\boldsymbol{u}}_c-\boldsymbol{s}^T(t_k)\hat{b}Tanh\left[\rho\boldsymbol{s}(t_k)\right]\\ &\leq \frac{\theta_1}{\theta}\left(b^2-\widetilde{b}^2\right)+\left(\alpha\hat{b}\beta_1-b\right)\|\boldsymbol{s}\|\\ &+\hat{b}\beta_1\gamma+\boldsymbol{s}^T(t_k)\bar{\boldsymbol{u}}_c+\frac{3\kappa\hat{b}}{\rho}\end{aligned} \tag{44}$$

From the characteristics of the neural network (6), $L_1\|\boldsymbol{s}\|$ meets the following inequation:

$$\begin{aligned}L_1\|\boldsymbol{s}\| &\leq \left[\boldsymbol{W}^T\boldsymbol{\phi}(\|\boldsymbol{\omega}\|)+\delta(\|\boldsymbol{\omega}\|)\right]\|\boldsymbol{s}\|\\ &\leq \boldsymbol{W}^T\boldsymbol{\phi}(\|\boldsymbol{\omega}\|)\|\boldsymbol{s}\|+\varepsilon_0\|\boldsymbol{s}\|\end{aligned} \tag{45}$$

where $\varepsilon_0 > 0$ is a small constant. According to (22), *Lemma 3* and Assumption 4, it's plausible to transform (45) into the inequation shown below:

$$\begin{aligned}L_1\|\boldsymbol{s}\| \leq\ & \left[\widetilde{\boldsymbol{W}}^{\,T}\boldsymbol{\phi}(\|\boldsymbol{\omega}\|)+\varepsilon_0+l\hat{\boldsymbol{W}}^T\boldsymbol{\phi}(\|\boldsymbol{\omega}-\boldsymbol{\omega}(t_k)\|)\right]\|\boldsymbol{s}\|\\ &+\boldsymbol{s}^T(t_k)\bar{\boldsymbol{u}}_b+\hat{\boldsymbol{W}}^T\boldsymbol{\phi}(\|\boldsymbol{\omega}(t_k)\|)\beta_1(\alpha\|\boldsymbol{s}\|+\gamma)+3\kappa/\eta\end{aligned} \tag{46}$$

Substituting (44)(46) into (43) leads to

$$\begin{aligned}\dot{V}_f \leq\ & -\left[\boldsymbol{s}-\boldsymbol{s}(t_k)\right]^T\left(\bar{\boldsymbol{u}}_a+\bar{\boldsymbol{u}}_b+\bar{\boldsymbol{u}}_c\right)+\boldsymbol{s}^T\left(\bar{\boldsymbol{u}}_a+\bar{\boldsymbol{u}}_b+\bar{\boldsymbol{u}}_c\right)\\ &-\boldsymbol{s}^T\boldsymbol{G}(\boldsymbol{\chi})^D\left(\bar{\boldsymbol{u}}_a+\bar{\boldsymbol{u}}_b+\bar{\boldsymbol{u}}_c\right)-\boldsymbol{s}^T(t_k)\bar{\boldsymbol{u}}_a+d_{max}\|\boldsymbol{s}\|\\ &+L_2\|\boldsymbol{s}\|+\frac{\theta_1}{\theta}\left(b^2-\widetilde{b}^2\right)-b\|\boldsymbol{s}\|+\hat{b}\beta_1(\alpha\|\boldsymbol{s}\|+\gamma)\\ &+\frac{3\kappa\hat{b}}{\rho}+\frac{3\kappa}{\eta}+\varepsilon_0\|\boldsymbol{s}\|+\hat{\boldsymbol{W}}^T\boldsymbol{\phi}(\|\boldsymbol{\omega}(t_k)\|)\beta_1(\alpha\|\boldsymbol{s}\|+\gamma)\\ &+\widetilde{\boldsymbol{W}}^{\,T}\boldsymbol{\phi}(\|\boldsymbol{\omega}\|)\|\boldsymbol{s}\|+l\hat{\boldsymbol{W}}^T\boldsymbol{\phi}(\|\boldsymbol{\omega}-\boldsymbol{\omega}(t_k)\|)\|\boldsymbol{s}\|\end{aligned} \tag{47}$$

where

$$\boldsymbol{s}^T\left[\boldsymbol{I}-\boldsymbol{G}(\boldsymbol{\chi})^D\right]\bar{\boldsymbol{u}} = \frac{1}{\varphi}\sum_{i=1}^{3}\dot{\chi}_i-\frac{1}{\varphi}\sum_{i=1}^{3}G(\chi_i)\dot{\chi}_i \tag{48}$$

Substituting (48) into (47) leads to

$$\begin{aligned}\dot{V}_f \leq\ & -\boldsymbol{e}^T\bar{\boldsymbol{u}}+\frac{1}{\varphi}\sum_{i=1}^{3}\dot{\chi}_i-\frac{1}{\varphi}\sum_{i=1}^{3}G(\chi_i)\dot{\chi}_i-k_2\left(\|\boldsymbol{s}-\boldsymbol{e}\|\right)^2\\ &+d_{max}\|\boldsymbol{s}\|+L_2\|\boldsymbol{s}\|+\frac{\theta_1}{\theta}\left(b^2-\widetilde{b}^2\right)+\hat{b}\beta_1(\alpha\|\boldsymbol{s}\|+\gamma)\\ &-b\|\boldsymbol{s}\|+\frac{3\kappa\hat{b}}{\rho}+\frac{3\kappa}{\eta}+\|\widetilde{\boldsymbol{W}}\|\phi_M\|\boldsymbol{s}\|+\varepsilon_0\|\boldsymbol{s}\|\\ &+\left(W_M+\|\widetilde{\boldsymbol{W}}\|\right)\phi_M\left[(l+\alpha\beta_1)\|\boldsymbol{s}\|+\beta_1\gamma\right]\end{aligned} \tag{49}$$

where

$$\begin{aligned}-k_2\left(\|\boldsymbol{s}-\boldsymbol{e}\|\right)^2 &\leq -k_2\left(\|\boldsymbol{s}\|-\|\boldsymbol{e}\|\right)^2\\ &\leq -\left(1-2\alpha\beta_1\right)k_2\|\boldsymbol{s}\|^2+2k_2\beta_1\gamma\|\boldsymbol{s}\|\end{aligned} \tag{50}$$

$$-\boldsymbol{e}^T\bar{\boldsymbol{u}} \leq \beta_1(\alpha\|\boldsymbol{s}\|+\gamma)\left[k_2\|\boldsymbol{s}\|+\left(W_M+\|\widetilde{\boldsymbol{W}}\|\right)\phi_M+\hat{b}\right] \tag{51}$$

From (50)(51), (49) can be rewritten as

$$\begin{aligned}\dot{V}_f \leq\ & \frac{1}{\varphi}\sum_{i=1}^{3}\dot{\chi}_i-\frac{1}{\varphi}\sum_{i=1}^{3}G(\chi_i)\dot{\chi}_i-\frac{V_f}{2\theta}\\ &-A\|\boldsymbol{s}\|^2+B\|\boldsymbol{s}\|+C-\frac{B^2}{4A}+\frac{B^2}{4A}\end{aligned} \tag{52}$$

where

$$\begin{cases} A = k_2\left(1-3\alpha\beta_1\right)-\theta_1 J_{max} \\ B = 2\alpha\beta_1\hat{b}+d_{max}+\varepsilon_0-b+\|\widetilde{\boldsymbol{W}}\|\phi_M \\ +\left(2\alpha\beta_1+l\right)\left(W_M+\|\widetilde{\boldsymbol{W}}\|\right)\phi_M+L_2 \\ C = 2\theta_1\|\widetilde{\boldsymbol{W}}\|^2+\frac{\theta_1}{\theta}b^2+\frac{3\kappa\hat{b}}{\rho}+\frac{3\kappa}{\eta} \\ +2\beta_1\gamma\left[\left(W_M+\|\widetilde{\boldsymbol{W}}\|\right)\phi_M+\hat{b}\right] \end{cases} \tag{53}$$

(52) can be rewritten as

$$\dot{V}_f \le \frac{1}{\varphi}\sum_{i=1}^{3}\dot{\chi}_i-\frac{1}{\varphi}\sum_{i=1}^{3}G\left(\chi_i\right)\dot{\chi}_i-\frac{V_f}{2\theta}+\frac{B^2}{4A}+C \tag{54}$$

Solve the differential inequation (54) and acquire

$$\begin{aligned} V_f\left(t\right) \le & -e^{-\frac{t}{2\theta}}\frac{1}{\varphi}\int_0^t\sum_{i=1}^{3}\left[G\left(\chi_i\right)-1\right]\dot{\chi}_i e^{\frac{\tau}{2\theta}}d\tau \\ & +e^{-\frac{t}{2\theta}}\left[V_f\left(0\right)-2\theta\left(\frac{B^2}{4A}+C\right)\right]+2\theta\left(\frac{B^2}{4A}+C\right) \end{aligned} \tag{55}$$

where scalar $2\theta\left(\frac{B^2}{4A}+C\right) > 0$, and $e^{-\frac{t}{2\theta}}\left[V_f\left(0\right)-2\theta\left(\frac{B^2}{4A}+C\right)\right]$ is a bounded time-varying function. Thus, $e^{-\frac{t}{2\theta}}\left[V_f\left(0\right)-2\theta\left(\frac{B^2}{4A}+C\right)\right]+2\theta\left(\frac{B^2}{4A}+C\right)$ is a bounded function that satisfies the applying situation of *Lemma 4*. From *Lemma 4*, $\chi_1\left(t\right),\chi_2\left(t\right),\chi_3\left(t\right),V_f\left(t\right)e^{-\frac{t}{2\theta}}\int_0^t\frac{1}{\varphi}\sum_{i=1}^{3}G\left(\chi_i\right)\dot{\chi}_i e^{\frac{\tau}{2\theta}}d\tau$, and $e^{-\frac{t}{2\theta}}\int_0^t\frac{1}{\varphi}\sum_{i=1}^{3}\dot{\chi}_i e^{\frac{\tau}{2\theta}}d\tau$ are all bounded on $[0\ ,+\infty)$. Consequently, $V_f\left(t\right)$ is upper bounded on $[0\ ,+\infty)$ and $V_f\left(t\right)$ always follows $V_f\left(t\right)\le V_M$, where $V_M>0$ is a constant. Correspondingly, $\chi_1\left(t\right),\chi_2\left(t\right),\chi_3\left(t\right)$ also follow $\chi_i\left(t\right)\le\ \chi_M, i=1,2,3$ for any $t>0$, where $\chi_M>0$ is a constant. Thus, during the flowing period, the Lyapunov function candidate follows

$$V_f=\widetilde{\boldsymbol{W}}^T\left(t\right)\widetilde{\boldsymbol{W}}\left(t\right)+\frac{1}{2}\boldsymbol{s}^T\boldsymbol{J}\boldsymbol{s}+\frac{1}{2\theta}\widetilde{b}^2\le V_M \tag{56}$$

(56) implies

$$\|\boldsymbol{s}\left(t\right)\|\le\sqrt{2V_M/J_{min}},\left\|\widetilde{b}\left(t\right)\right\|\le\sqrt{2V_M\theta},t>0 \tag{57}$$

Thus, both the adaptive parameter $\hat{b}$ and the sliding mode vector $\boldsymbol{s}\left(t\right)$ are ultimately bounded during the flowing period. From [25], the ultimate boundedness of $\boldsymbol{s}\left(t\right)$ decides the ultimate boundedness of $\boldsymbol{\omega}_e,\boldsymbol{q}_{v,e},\boldsymbol{\omega},\boldsymbol{q}_v$ during the flowing period. Considering that *Theorem 1* has substantiated the ultimate boundedness of $\widetilde{\boldsymbol{W}}\left(t\right)$. It's plausible to draw the conclusion that all the system signals are ultimately bound during the flowing period.

Furthermore, it's reasonable to substantiate that all the system signals will converge to zero during the flowing period by the following proof. From (27)(29),

$$\dot{\chi}_i=\varphi s_i\bar{u}_i\ge\varphi k s_i^2 \tag{58}$$

Integrating (58) leads to

$$\varphi k\int_0^t\boldsymbol{s}^T\left(\tau\right)\boldsymbol{s}\left(\tau\right)d\tau\le\ \chi_i\left(t\right)-\ \chi_i\left(0\right)\le\ \chi_M \tag{59}$$

(59) implies that $\int_0^t\boldsymbol{s}^T\left(\tau\right)\boldsymbol{s}\left(\tau\right)d\tau$ is bounded on $\tau\in[0,t)$. Moreover, (13) shows that $\boldsymbol{s}^T\left(\tau\right)\dot{\boldsymbol{s}}\left(\tau\right)$ exists on $\tau\in[0,t)$, implying that $\boldsymbol{s}^T\left(\tau\right)\boldsymbol{s}\left(\tau\right)$ is uniformly continuous. According to *Lemma 2* Barbalats lemma, consider that $\lim_{t\to\infty}\boldsymbol{s}^T\left(t\right)\boldsymbol{s}\left(t\right)=\chi_M/\varphi k$ is finite and $2\boldsymbol{s}^T\left(\tau\right)\dot{\boldsymbol{s}}\left(\tau\right)$ is uniformly continuous, it's logical to draw the conclusion that

$$\lim_{t\to\infty}\|\boldsymbol{s}\left(t\right)\|=0 \tag{60}$$

This part of the proof augments the effectiveness of *Theorem 2* during the flowing period.

Case 2 (Jumping dynamics,$t=t_k,\ k=1,2,\ldots$):

It's reasonable to select the following Lyapunov candidate function for stability analysis at the triggering instants:

$$\begin{aligned} V_J &= V_{s(t_k)}+V_{\widetilde{W}}+V_{\widetilde{b}}+V_{\boldsymbol{\chi}} \\ &= \boldsymbol{s}^T\left(t_k\right)\boldsymbol{s}\left(t_k\right)+\widetilde{\boldsymbol{W}}^T\widetilde{\boldsymbol{W}}+\widetilde{b}^T\widetilde{b}+\boldsymbol{\chi}^T\boldsymbol{\chi} \end{aligned} \tag{61}$$

The first derivative of (61) is

$$\begin{aligned} \Delta V_J &= \left\|\boldsymbol{s}^+\right\|^2-\|\boldsymbol{s}\left(t_{k-1}\right)\|^2+\widetilde{b}^{+2}-\widetilde{b}^2+\left\|\widetilde{\boldsymbol{W}}^+\right\|^2-\|\widetilde{\boldsymbol{W}}\|^2 \\ &+\left\|\boldsymbol{\chi}^+\right\|^2-\|\boldsymbol{\chi}\|^2\le-\|\widetilde{\boldsymbol{W}}\|^2-\|\boldsymbol{s}-\boldsymbol{e}\|^2-\widetilde{b}^2\left(t_{k-1}\right)+D \end{aligned} \tag{62}$$

where D represents the maximum value of $\|\widetilde{\boldsymbol{W}}\|^2+\|\boldsymbol{s}\|^2+\widetilde{b}^2+\chi_M^2$ during the flowing period, considering that $\|\widetilde{\boldsymbol{W}}\|,\|\boldsymbol{s}\|,\widetilde{b},\|\boldsymbol{\chi}\|$ are all upper bounded during the flowing period, it's reasonable to make sure that all the system signals are bounded at the triggering instants.

Summarize the analysis in case 1 and case 2. It's reasonable to conclude that all the signals in the proposed control system are ultimately bounded. ■

C. Zeno analysis

Zeno behavior denotes the situation where the event-triggered mechanism is triggered infinite times in a finite amount of time [25]. It's necessary to carry out Zeno analysis to thoroughly exclude Zeno behavior. Furthermore, Zeno analysis is also an approach to estimating the MIET, which could reveal the inner logic of the proposed sigmoid event-triggered mechanism. The following theorem will expose the secret of high MIET.

Theorem 3: Consider the attitude tracking model of a spacecraft (1-3), with *Lemma 1-4*, inequation(17), the adaptive update algorithm of NN (23)(24), the "augmented precision" adaptive law (26), the dynamic-loop gain adaptive law (29), the high MIET event-triggered mechanism (33)(34), *Theorem 1* and *Theorem 2*. If Assumptions 1-4 hold and the control law (27)(28) is implemented, then it's reasonable to delude the MIET follows:

$$T_{min}\ge\frac{\ln\left\{\frac{Y}{Z}\beta_1\left[\alpha\left(\boldsymbol{s}\left\|t_{k+1}\right\|\right)+\gamma\right]\right\}+1}{Y} \tag{63}$$

where

$$\begin{cases} Y = \frac{1}{J_{min}} \left[k_2 \left\| \boldsymbol{G}(\boldsymbol{\chi})^D \right\| + 2\frac{\left(W_M + \|\widetilde{\boldsymbol{W}}\|\right)\phi_M}{\|\boldsymbol{s}\|} \right] \\ Z = \frac{1}{J_{min}} \left[\left(W_M + \|\widetilde{\boldsymbol{W}}\|\right)\phi_M + k_2 \left\| \boldsymbol{G}(\boldsymbol{\chi})^D \right\| \|\boldsymbol{s}\| \right. \\ + \left\| G(\boldsymbol{\chi})^D \right\| \left(W_M + \|\widetilde{\boldsymbol{W}}\|\right)\phi_M + \varepsilon_0 + \left\| G(\boldsymbol{\chi})^D \right\| \hat{b} \\ \left. + d_{max} + \|\widetilde{\boldsymbol{W}}\|\phi_M + l\left(W_M + \left\|\widetilde{\boldsymbol{W}}\right\|\right)\phi_M + \frac{3\kappa}{\eta\|\boldsymbol{s}\|} \right] \end{cases} \tag{64}$$

Proof: Consider the following inequation:

$$\frac{d}{dt}\|\boldsymbol{e}\| = \frac{d}{dt}\sqrt{\boldsymbol{e}^T\boldsymbol{e}} = \frac{\boldsymbol{e}^T\dot{\boldsymbol{e}}}{\|\boldsymbol{e}\|} \le \left\|\dot{\boldsymbol{e}}\right\| = \left\|\dot{\boldsymbol{s}}\right\| \le \frac{\left\|\boldsymbol{J}\dot{\boldsymbol{s}}\right\|}{J_{min}} \tag{65}$$

where $\left\|\boldsymbol{J}\dot{\boldsymbol{s}}\right\|$ follows

$$\begin{aligned} &\left\|\boldsymbol{J}\dot{\boldsymbol{s}}\right\| \le \left\|\bar{\boldsymbol{u}}_b\right\| + \left\|\boldsymbol{G}(\boldsymbol{\chi})^D\left(\bar{\boldsymbol{u}}_a + \bar{\boldsymbol{u}}_b + \bar{\boldsymbol{u}}_c\right)\right\| + d_{max} \\ &+ \varepsilon_0 + \left|\widetilde{\boldsymbol{W}}^T\boldsymbol{\phi}(\|\boldsymbol{\omega}\|)\right| + \left|l\hat{\boldsymbol{W}}^T\boldsymbol{\phi}(\|\boldsymbol{\omega} - \boldsymbol{\omega}(t_k)\|)\right| + \frac{3\kappa}{\eta\|\boldsymbol{s}\|} \\ &+ \frac{\boldsymbol{e}^T\bar{\boldsymbol{u}}_b + \hat{\boldsymbol{W}}^T\boldsymbol{\phi}(\|\boldsymbol{\omega}(t_k)\|)\|\boldsymbol{e}\|}{\|\boldsymbol{s}\|} \le J_{min}(Y\|\boldsymbol{e}\| + Z) \end{aligned} \tag{66}$$

Substituting (64)(66) into (65) leads to

$$\frac{d}{dt}\|\boldsymbol{e}\| \le Y\|\boldsymbol{e}\| + Z \tag{67}$$

At the triggering instants, $\|\boldsymbol{e}\|_{t=t_k} = 0$. Consider that and then solve the inequation (67) results in

$$\|\boldsymbol{e}\| \le \frac{Z}{Y} exp\left[Y(t - t_k) - 1\right] \tag{68}$$

At the triggering instants, there exists $\|\boldsymbol{e}(t_{k+1})\| = \beta_1\left[\alpha\|\boldsymbol{s}(t_{k+1})\| + \gamma\right]$. It's rational to rewrite (68) as follows:

$$\beta_1\left(\alpha\|\boldsymbol{s}(t_{k+1})\| + \gamma\right) \le \frac{Z}{Y} exp\left[Y(t_{k+1} - t_k) - 1\right] \tag{69}$$

Then it's reasonable to transform (69) into the following inequation:

$$t_{k+1} - t_k \ge \frac{\ln\left[\frac{Y}{Z}\beta_1\left(\alpha\|\boldsymbol{s}(t_{k+1})\| + \gamma\right)\right] + 1}{Y} \tag{70}$$

Hence,

$$T_{min} \ge \frac{\ln\left[\frac{Y}{Z}\beta_1\left(\alpha\|\boldsymbol{s}(t_{k+1})\| + \gamma\right)\right] + 1}{Y} \tag{71}$$

where $Y > 0, Z > 0$ are finite constants since all the system signals are ultimately bounded due to *Theorem 2*. Besides, $\beta_1 = 1 + c_1 - c_1 tanh\left(\frac{\mu_1}{k_1\left\|\boldsymbol{q}_{v,e}\right\| + \|\boldsymbol{\omega}_e\|}\right)$ and $\|\boldsymbol{s}(t_{k+1})\|$ are also upper bounded since $\|\boldsymbol{s}\|, \left\|\boldsymbol{q}_{v,e}\right\|, \|\boldsymbol{\omega}_e\|$ are all upper-bounded. Thus, the proposed high MIET event-triggered mechanism can avoid any Zeno behavior, and the following analysis can reveal the core logic of high MIET:

D. The core logic of high inter-execution time

Substituting (34) into (71) leads to

$$\begin{aligned} T_{min} \ge{}& \frac{1}{Y}\left\{\ln\left[\frac{Y\left[\alpha(\boldsymbol{s}) + \gamma\right]}{Z}\right] + 1\right\} \\ &+ \frac{1}{Y}\ln\left[1 + c_1 - c_1 tanh\left(\frac{\mu_1}{k_1\left\|\boldsymbol{q}_{v,e}\right\| + \|\boldsymbol{\omega}_e\|}\right)\right] \end{aligned} \tag{72}$$

where $\beta_1 = 1 + c_1 - c_1 tanh\left(\frac{\mu_1}{k_1\left\|\boldsymbol{q}_{v,e}\right\| + \|\boldsymbol{\omega}_e\|}\right)$ improves the lower bound of MIET significantly. According to the theory of control and experience of numerical simulation, the overshoot $\|\boldsymbol{s}\|$ varies sharply at the initial stage of attitude tracking, which means the event-triggered mechanism with the following MIET:

$$T'_{min} \ge \frac{\ln\left[\frac{Y}{Z}\left(\alpha\|\boldsymbol{s}\| + \gamma\right)\right] + 1}{Y} \tag{73}$$

will be frequently triggered. Because $\alpha > 0, \gamma > 0$ are minor constants, and the decrease of $\|\boldsymbol{s}\|$ will also result in the decrease of $\frac{1}{Y}$, which will further minimize the lower bound of MIET.

In comparison to the traditional event-triggered mechanism whose MIET is shown as (73), the proposed sigmoid event-triggered mechanism can hamper the rapid variation of $\alpha\|\boldsymbol{s}\| + \gamma$ at the initial stage of attitude tracking effectively. This is due to the introduction of the term $\beta_1 = 1 + c_1 - c_1 tanh\left(\frac{\mu_1}{k_1\left\|\boldsymbol{q}_{v,e}\right\| + \|\boldsymbol{\omega}_e\|}\right)$ in (33).

At the initial stage of attitude tracking, the overshoot $\|\boldsymbol{s}\|$ may be very high. A decrease in $\|\boldsymbol{s}\|$ results in a decrease in $k_1\left\|\boldsymbol{q}_{v,e}\right\| + \|\boldsymbol{\omega}_e\|$, and a decrease in $k_1\left\|\boldsymbol{q}_{v,e}\right\| + \|\boldsymbol{\omega}_e\|$ leads to a booming increase in $\beta_1 = 1 + c_1 - c_1 tanh\left(\frac{\mu_1}{k_1\left\|\boldsymbol{q}_{v,e}\right\| + \|\boldsymbol{\omega}_e\|}\right)$. Consequently, unlike the term $\alpha\|\boldsymbol{s}\| + \gamma$, the term $\left[1 + c_1 - c_1 tanh\left(\frac{\mu_1}{k_1\left\|\boldsymbol{q}_{v,e}\right\| + \|\boldsymbol{\omega}_e\|}\right)\right](\alpha\|\boldsymbol{s}\| + \gamma)$ can stabilize over a much higher lower bound, reducing the possibility of frequent, consistent triggering events in a short time.

Besides, rather than $\|\boldsymbol{s}\|$, the denominator in the hyperbolic tangent function must be set as $k_1\left\|\boldsymbol{q}_{v,e}\right\| + \|\boldsymbol{\omega}_e\|$. Because the three components of $\boldsymbol{q}_{v,e}$ and those of $\boldsymbol{\omega}_e$ always present the opposite character of plus-minus. Therefore, $\|\boldsymbol{s}\| = \left\|k_1\boldsymbol{q}_{v,e} + \boldsymbol{\omega}_e\right\|$ is always close to zero. $\|\boldsymbol{s}\| \approx 0$ means $\beta_1 \approx 0$, so $\|\boldsymbol{s}\| \approx 0$ may bring the event-triggered mechanism with $\beta_1 = 1 + c_1 - c_1 tanh\left(\frac{\mu_1}{\|\boldsymbol{s}\|}\right)$ to high risk of frequent, consistent triggering events again. By contrast, both the control theory and the numerical simulation demonstrate that $k_1\left\|\boldsymbol{q}_{v,e}\right\| + \|\boldsymbol{\omega}_e\|$ decreases smoothly without sharply increasing, which means $k_1\left\|\boldsymbol{q}_{v,e}\right\| + \|\boldsymbol{\omega}_e\|$ is an ideal candidate for the denominator.

Furthermore, $\|\boldsymbol{s}\| = 0$ means $\alpha\|\boldsymbol{s}\| + \gamma = \gamma$. Thus, $\|\boldsymbol{s}\| = 0$ implies the maximum possibility of network congestion for any event-triggered control system with its minimum inter-execution time expressed like that in (73), which is given as follows:

$$T'_{MIET} \approx \frac{\ln\left(\frac{Y}{Z}\gamma\right) + 1}{Y} \tag{74}$$

In contrast, at the beginning of tracking or when the states $\left\|\boldsymbol{q}_{v,e}\right\|$ or $\|\boldsymbol{\omega}_e\|$ are high, the application of the term β_1 to the proposed event-triggered mechanism (33) can result in a much higher theoretical minimum inter-execution time expressed as follows:

$$T_{MIET} \approx \frac{\ln\left[\left(1+c_1^{'}\right)\frac{Y}{Z}\gamma\right]+1}{Y} \tag{75}$$

where $c_1^{'} > 0$ can be very high as long as suitable $c_1\mu_1$ have been selected. Note that $\beta_1 = 1 + c_1 - c_1 tanh\left(\frac{\mu_1}{k_1\left\|\boldsymbol{q}_{v,e}\right\|+\|\boldsymbol{\omega}_e\|}\right)$. If c_1 and μ_1 have been chosen, then higher $\left\|\boldsymbol{q}_{v,e}\right\|$ and higher $\|\boldsymbol{\omega}_e\|$, also can be seen as higher $\|\boldsymbol{s}\| = \left\|\boldsymbol{\omega}_e + k_1\boldsymbol{q}_{v,e}\right\|$, will inevitably lead to higher $c_1^{'}$. According to a traditional event-triggered mechanism without the term β_1 as follows:

$$t_{k+1} = min\left\{t \geq t_k : \|\boldsymbol{e}\| \geq \alpha\|\boldsymbol{s}\| + \gamma\right\}, k = 0, 1, \ldots \tag{76}$$

Higher $\|\boldsymbol{s}\|$ always implies a higher possibility of triggering, which also always implies a higher risk of network congestion. Because $\|\boldsymbol{e}\| = \|\boldsymbol{s}\| - \|\boldsymbol{s}\left(t_k\right)\|$ and the ETM will be triggered when

$$\|\boldsymbol{s}\| \geq \frac{\|\boldsymbol{s}\left(t_k\right)\| + \gamma}{1-\alpha} \tag{77}$$

Thus, it's reasonable to claim that the proposed sigmoid ETM can improve the theoretical minimum inter-execution time the most at the instants with the highest risk of network congestion. Besides, the time difference between (74) and (75) is

$$\begin{aligned} T_{ADD} &= T_{MIET} - T_{MIET}^{'} \\ &\approx \frac{\ln\left[\left(1+c_1^{'}\right)\frac{Y}{Z}\gamma\right] - ln\left(\frac{Y}{Z}\gamma\right)}{Y} = \frac{ln\left(1+c_1^{'}\right)}{Y} \end{aligned} \tag{78}$$

(78) can demonstrate that the proposed event-triggered control scheme is much better than any previous network control system in improving the MIET.

Moreover, the proposed event-triggered mechanism with the term β_1 not only improves the MIET efficiently but also improves the mean inter-execution time. Compared with the previous event-triggered mechanisms without the term β_1, the ratio of the maximum inter-execution time to the minimum inter-execution time is much smaller in this paper. A much lower maximum-to-minimum ratio is beneficial for making full use of limited resources for communication.It is also much better in decreasing the cost of wireless networks on the premise of the same requirement for attitude tracking precision.

Remark 4: Different from all kinds of known event-triggered mechanisms, the variable structure term β_1 is added in the sigmoid ETM, which endows the sigmoid ETM with the ability to avoid highly uneven distribution of the triggering instants on the timeline. Thanks to the mapping function of sigmoid functions like the hyperbolic tangent function, by increasing the variable structure term β_1 to almost $1 + c_1$ promptly, it's viable to relax the sigmoid event-triggered condition to avoid frequent triggering events when the control overshot is very high. Correspondingly, μ_1 should be much smaller than the theoretical maximum value of $k_1\left\|\boldsymbol{q}_{v,e}\right\| + \|\boldsymbol{\omega}_e\|$. For simplicity, μ_1 should not exceed 1/5 of $k_1\left\|\boldsymbol{q}_{v,e}\right\| + \|\boldsymbol{\omega}_e\|$ at the initial moment. By contrast, to ensure precise attitude tracking at the steady-state, it's necessary to tighten the event-triggered condition by decreasing β_1 to about 1. Thus, parameter μ_1 should be higher than the expected $k_1\left\|\boldsymbol{q}_{v,e}\right\| + \|\boldsymbol{\omega}_e\|$ at steady-state. As for parameter c_1, a parameter c_1 that much larger than 1 is acceptable on the premise of not lowering the accuracy of attitude tracking or resulting in control divergence. Similar to traditional event-triggered control, $\alpha, \gamma > 0$ decide the frequency of wireless data transmission when the control system is in a steady-state situation. The higher α or $\gamma > 0$ will result in a looser sigmoid ETM which is much easier to be triggered, so it's reasonable to select minor α, $\gamma > 0$ no more than 0.01 to avoid frequent wireless communication.

V. Numerical Simulation

In this section, numerical simulations are implemented to verify the proposed high MIET event-triggered control scheme. It's reasonable to choose a spacecraft with the following inertia matrix [24]:

$$\boldsymbol{J} = \begin{bmatrix} 132 & 6 & 5 \\ 6 & 126 & 7 \\ 5 & 7 & 141 \end{bmatrix} kg \cdot m^2 \tag{79}$$

Consider the influence of gravitation, solar radiation pressure, aerodynamic drag, and magnetic forces. It's rational to set the external disturbance as follows:

$$\boldsymbol{d} = \begin{bmatrix} 1 + 2\sin 0.5t \\ -1 - 5\sin 0.5t \\ 2 + 4\ cos\ 0.5t \end{bmatrix} \times 10^{-4} N \cdot m \tag{80}$$

Besides, it's rational to assume that the torque distribution system can allocate no more than $0.5Nm$ to each axis of the body frame of a spacecraft. The initial attitude tracking errors are assumed as $\boldsymbol{q}_{v,\ e0} = \left[\sin\left(3^{\circ}\right) \quad -\sin\left(2.5^{\circ}\right) \quad \sin\left(4^{\circ}\right)\right]^T$, and the initial attitude angular velocity errors are assumed as $\boldsymbol{\omega}_{e0} = \left[0.01 \quad -0.01 \quad -0.01\right]^T deg/s$. In addition, the desired attitude tracking errors are set to $\boldsymbol{q}_{v,d} = \left[0 \quad 0 \quad 0\right]^T$, and the desired attitude angular velocity errors are assumed to be $\boldsymbol{\omega}_d = \left[0.375sin\left(\pi t/100\right) \quad 0.125sin\left(\pi t/100\right) \quad 0.175cos\left(\pi t/100\right)\right]^T deg/s$.

What's more, the control gain is chosen as $k_2 = 23.62$, and the sliding-mode parameter is selected as $k_1 = 0.451$. As for the neural networks, the basis functions are selected as Gaussian functions with 11 nodes. The centers of these 11 nodes are evenly distributed in $[-0.5, 0.5]$, and their widths are all 1. The neural networks' adaptive parameters are chosen as $\sigma = 0.0018, \beta = 2, c = 2$. The reflective parameter in the neural networks is selected as $\eta = 200$. When $t = 0$, $\hat{\boldsymbol{W}}\left(0\right) = 0$, where $\hat{\boldsymbol{W}}$ is a 11×1 vector. Correspondingly, the basis function $\boldsymbol{\phi}$ is also a 11×1 vector. Similar to the neural networks, in the "augmented precision" adaptive law, $\hat{b}\left(0\right) = 0$, the adaptive parameters are selected as $\theta = 143, \theta_1 = 0.00205$, and the reflective parameter is chosen as $\rho = 22$. In addition, the dynamic-loop gain parameters are chosen as $\chi_1\left(0\right) = 0.675, \chi_2\left(0\right) = 0.67, \chi_3\left(0\right) = 0.665, \varphi =$

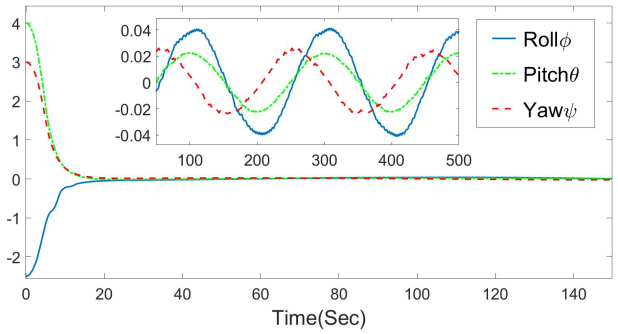

Fig. 3. Attitude tracking errors (Deg)

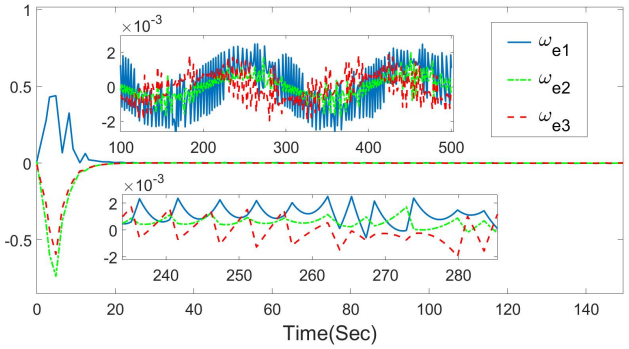

Fig. 4. Angular Velocity Tracking Errors (Deg/Sec)

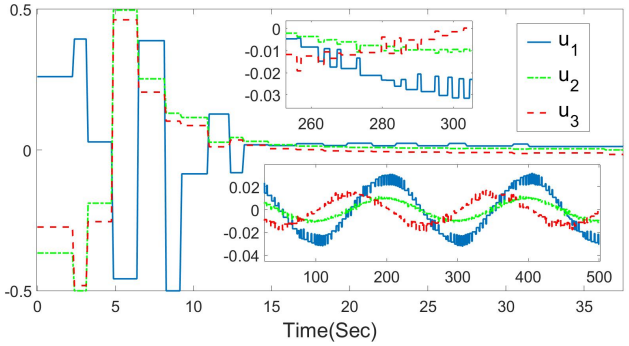

Fig. 5. Control Torques (Nm)

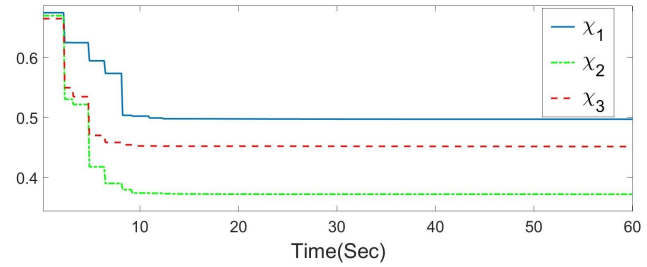

Fig. 6. Dynamic loop gain parameters χ_1, χ_2, and χ_3

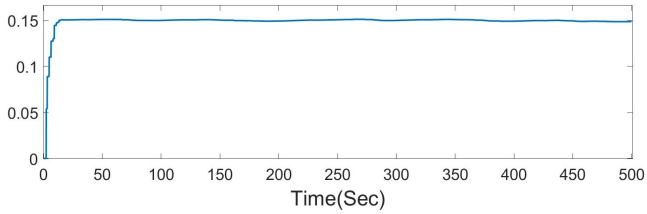

Fig. 7. The estimation of the NN $\|\hat{\boldsymbol{W}}\|$

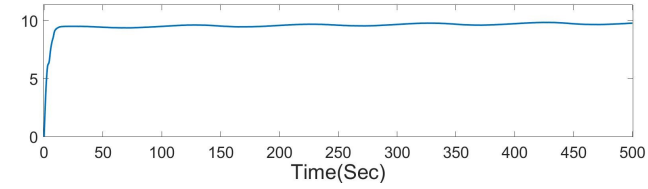

Fig. 8. Adaptive parameter $\hat{b}$

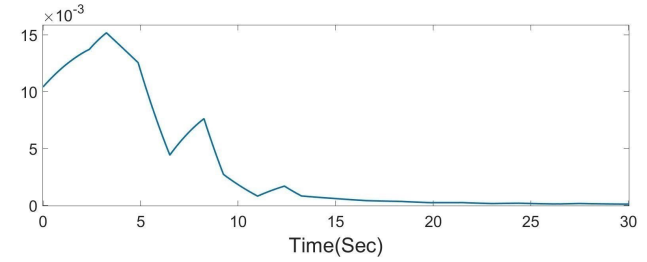

Fig. 9. $\|\boldsymbol{\omega}_e\| + k_1 \left\|\boldsymbol{q}_{v,e}\right\|$

162.35. Last and also the most important, the event-triggered parameters are selected as $\alpha = 0.01181, \gamma = 4.8 \times 10^{-5}, c_1 = 77, \mu_1 = 0.0024$.

The time length of the numerical simulation is 500 seconds, and the step size is 0.125 s. Fig. 3 demonstrates the attitude tracking errors. Fig. 4 illustrates the angular velocity tracking errors. Fig. 3 and Fig. 4 verify that errors converge within small bounds and that the proposed control system can cope with the mission of attitude takeover control with high precision.

Furthermore, Fig. 5 demonstrates the variation of control torques. Numerical simulation verifies that the proposed dynamic-loop gain approach can deal with the problem of input saturation effectively. Fig. 6 shows the variation of the dynamic-loop gain parameters, χ_1, χ_2, χ_3 converge to constants. Fig. 7 and Fig. 8 depict the variation of $\|\hat{\boldsymbol{W}}\|$ and $\hat{b}$, respectively. Both the estimation of the NN and the "augmented precision" adaptive parameter $\hat{b}$ are ultimately bounded. The variation of $k_1 \left\|\boldsymbol{q}_{v,e}\right\| + \|\boldsymbol{\omega}_e\|$ is depicted in Fig. 9. By contrast, Fig. 10 illustrates the variation of $\|\boldsymbol{s}\|$. In spite of frequent $\|\boldsymbol{s}\|$, the three components of $k_1 \left\|\boldsymbol{q}_{v,e}\right\| + \|\boldsymbol{\omega}_e\|$ decrease relatively monotonically, which confirms that $k_1 \left\|\boldsymbol{q}_{v,e}\right\| + \|\boldsymbol{\omega}_e\|$ is an appropriate denominator in $\beta_1 = 1 + c_1 - c_1 tanh\left(\frac{\mu_1}{k_1 \left\|\boldsymbol{q}_{v,e}\right\| + \|\boldsymbol{\omega}_e\|}\right)$. In contrast to $k_1 \left\|\boldsymbol{q}_{v,e}\right\| + \|\boldsymbol{\omega}_e\|$, $\|\boldsymbol{s}\|$ always passes $\|\boldsymbol{s}\| = 0$, resulting in the frequent unexpected variation of $\beta_1^{'} = 1 + c_1 - c_1 tanh\left(\frac{\mu_1}{\|\boldsymbol{s}\|}\right)$. Therefore, $\|\boldsymbol{s}\|$ is not an ideal variable to play the role of dominator in the proposed event-triggered mechanism.

Fig. 11 depicts the variation of the event-triggered condition.

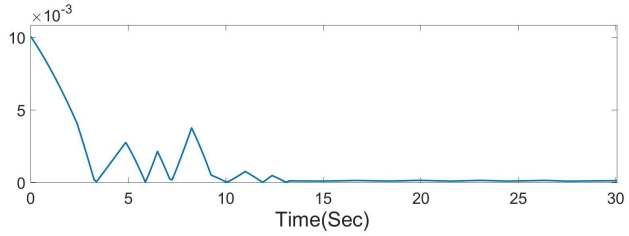

Fig. 10. $\|\mathbf{s}\| = \|\omega_e + k_1 \mathbf{q}_{v,e}\|$

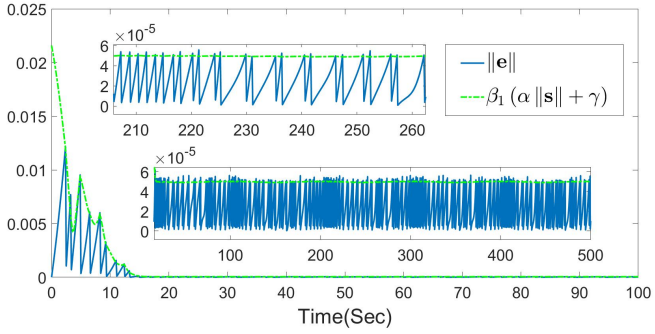

Fig. 11. Event-triggered condition

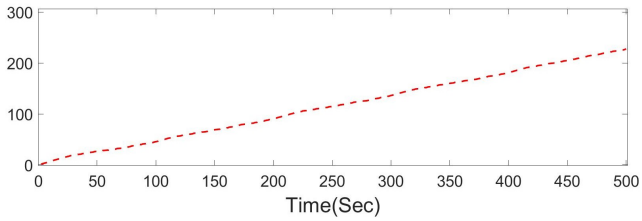

Fig. 12. Accumulated times of triggering

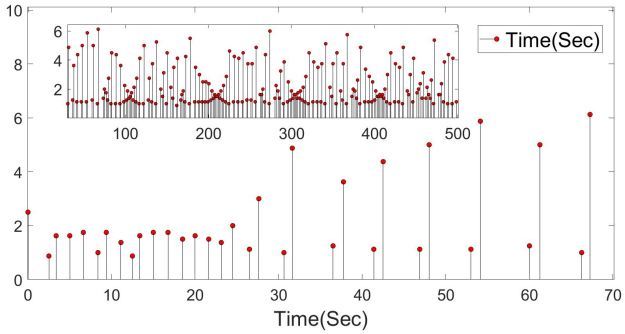

Fig. 13. Distribution of the inter-execution time with sigmoid ETM

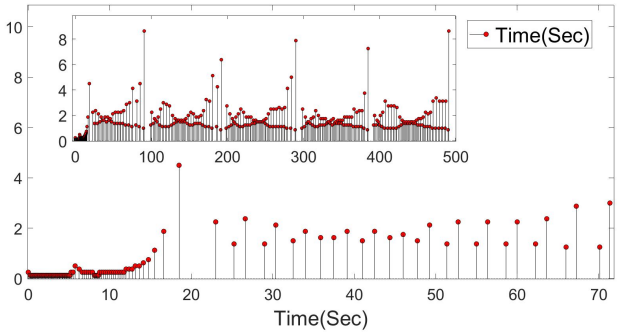

Fig. 14. Distribution of the inter-execution time with static ETM

The event-triggered condition $\beta_1 (\alpha \|\boldsymbol{s}\| + \gamma)$ decreases relatively monotonously, which is beneficial for reducing the ratio of minimum inter-execution time to mean inter-execution time. The inter-execution times and the distribution of triggering instants are presented in Fig. 12 and Fig. 13, respectively. The proposed sigmoid event-triggered mechanism has been triggered 228 times in 500 s. That's to say, the average inter-execution time is 2.193 s. Consider that the control frequency of a traditional attitude control system with equivalent control accuracy is required to be 8 Hz or even higher. The size of wireless communication is reduced by 94.3% with the help of the proposed high minimum IET event-triggered mechanism.

In contrast to the average inter-execution time, the minimum inter-execution time is 0.875 s, which means the ratio of the minimum inter-execution time to the average inter-execution time stands at 39.9%. By contrast, to realize attitude tracking, other event-triggered control schemes with the structure illustrated in Fig. 1 can only stand no more than 5% [24], [40], [43]. Consider that the direct comparison between the proposed sigmoid event-triggered method and other kinds of methods in the minimum inter-execution time may be unfair as a result of different controllers and many other factors. It's much fairer to hold a competition between the proposed sigmoid event-triggered mechanism and its own static version with $c_1 = 0$. Fig. 14 demonstrates the result of this fair duel between the sigmoid event-triggered control and the static event-triggered control. On the premise of the same ultimate attitude tracking errors and the same ultimate angular velocity tracking errors, the minimum inter-execution time resulted from the sigmoid one is 0.875 s, while this index led by the static one is 0.125 s. Obviously, the sigmoid one wins with an overwhelming advantage. Therefore, the proposed method can improve the minimum inter-execution time significantly. Meanwhile, the proposed scheme can reduce the possibility of network congestion, like time delay or package loss, a lot.

Remark 5: There is a $c_1 = 0$ that invalidates the variable structure term (34) and translates the sigmoid ETM into a common static ETM in order to generate Fig. 14. Furthermore, the design parameter μ_1 is reset as $\mu_1 = 0.00004$, and the dynamic-loop gain parameters are reset as $\chi_1(0) = 0.475, \chi_2(0) = 0.47, \chi_3(0) = 0.465, \varphi = 5.3, \mu_1 = 0.00004$. Except for the change in c_1, μ_1 and the dynamic-loop gain parameters, all the parameters are set the same in both the sigmoid event-triggered control scheme and its static version, which verifies the persuasion of the competition.

Besides, Fig. 15 and Fig. 16 demonstrate the attitude tracking errors and the angular velocity tracking errors obtained by replacing original $\bar{\boldsymbol{u}}$ in (27) with $\bar{\boldsymbol{u}} = k_2 \boldsymbol{s}(t_k) + \left|\hat{\boldsymbol{W}}^T \boldsymbol{\phi}(\|\boldsymbol{s}(t_k)\|)\right| Tanh\left[\eta \boldsymbol{s}(t_k) \hat{\boldsymbol{W}}^T \boldsymbol{\phi}(\|\boldsymbol{s}(t_k)\|)\right]$. These two figures have shown the most ideal ultimate attitude tracking errors and angular velocity errors by trying the best to tuning the parameters of control and event-triggering in the premise of keeping the original states of most of the simulation

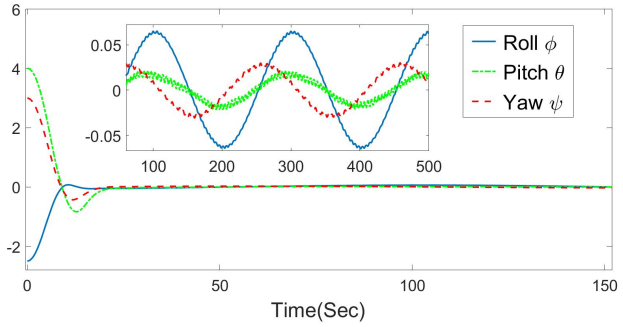

Fig. 15. Attitude tracking errors (Deg) without the additional adaptive algorithm (25) and (26)

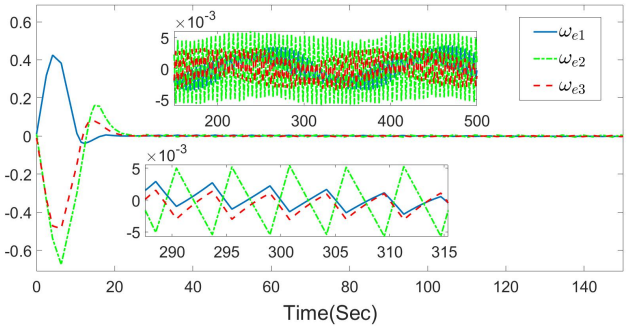

Fig. 16. Angular velocity tracking errors (Deg/Sec) without the additional adaptive algorithm (25) and (26)

parameters like the inertia matrix or the disturbances, and also persuing the results with high-performance in improving the MIET as Figs. 3 to 13 show.

On the premise of keeping the original states of most of the simulation parameters, like the inertia matrix or the disturbances, these two figures have shown the most ideal ultimate attitude tracking errors and angular velocity errors by selecting almost the perfect control parameters and event-triggered parameters to meet the target of improving the MIET as high as possible. As Figs. 15 and 16 illustrate, the ultimate bounds of errors are much bigger than those shown by Figs. 3 and 4. Even so, the MIET acquired after altering the control algorithm is just around 0.5 seconds, and any extra efforts to improve the MIET to 0.875 seconds as shown in Fig. 13 will only lead to greater ultimate errors in attitude tracking and angular velocity tracking. Thus, as Remark 2 said, it is much better to add an additional adaptive approximation term (25).

VI. Conclusions

This paper researches the problem of attitude tracking for spacecraft with limited communication, network congestion, unknown model parameters, actuator saturation, and external disturbances. To alleviate the communication load, a novel sigmoid event-triggered mechanism is proposed with its special ability to guarantee a high minimum inter-event time to decrease the possibility of network congestion like package loss or time delay effectively. A neural network-based adaptive control algorithm is designed to deal with unknown model parameters. Besides, the problem of actuator saturation is tackled by introducing a dynamic loop gain function-based approach. System stability is proved by Lyapunov stability analysis, and the high minimum inter-event time is substantiated by Zeno Behavior analysis with explanatory remarks. Numerical simulation results also show that a high minimum inter-event time and a high average inter-event time can be realized on the premise of high attitude tracking accuracy. The size of wireless communication is reduced by 94.3%. The minimum inter-execution time is 0.875 s, which is 7 times the step size of the numerical simulation. Furthermore, the ratio of the minimum inter-execution time to the average inter-execution time stands at 39.9%. By contrast, the previous studies could not increase the MIET effectively, and the corresponding ratio always stood at 5% or less, which demonstrates the huge progress brought by the proposed sigmoid event-triggered method.

References

[1] Hugh G. Lewis, "Understanding long-term orbital debris population dynamics," *Journal of Space Safety Engineering*, vol. 7, no. 3, pp. 164–170, 2020.

[2] M.P. Cartmell, D.J. McKenzie, "A review of space tether research," *Progress in Aerospace Sciences*, vol. 44, no. 1, pp. 1–21, 2008.

[3] Angel Flores-Abad, Ou Ma, Khanh Pham, Steve Ulrich, "A review of space robotics technologies for on-orbit servicing," *Progress in Aerospace Sciences*, vol. 68, no. 1, pp. 1–26, 2014.

[4] Tanaka, Hideyuki, "Reconfigurable cellular satellites maintained by space robots," *J. Robotics Mechatronics*, vol. 18, pp. 356–364, 2006.

[5] P. Huang, M. Wang, Z. Meng, F. Zhang, Z. Liu, "Attitude takeover control for post-capture of target spacecraft using space robot," *Aerospace Science and Technology*, vol. 51, pp. 171–180, 2016.

[6] P. Huang, M. Wang, Z. Meng, F. Zhang, Z. Liu, Haitao Chang, "Reconfigurable spacecraft attitude takeover control in post-capture of target by space manipulators," *Journal of the Franklin Institute*, vol. 353, no. 9, pp. 1985–2008, 2016.

[7] P. Huang, Y. Lu, M. Wang, Z. Meng, Y. Zhang and F. Zhang, "Post-capture Attitude Takeover Control of a Partially Failed Spacecraft With Parametric Uncertainties," *IEEE Transactions on Automation Science and Engineering*, vol. 16, no. 2, pp. 919–930, April 2019.

[8] D. Barnhart, B. Sullivan, and R. Hunter, "Phoenix program status-2013," in *AIAA SPACE 2013 conference and exposition*, 2013.

[9] Ahmed, Jasim, Vincent T. Coppola, and Dennis S. Bernstein. "Adaptive asymptotic tracking of spacecraft attitude motion with inertia matrix identification," *Journal of Guidance, Control, and Dynamics*, vol. 21, no. 5, pp. 684–691, 1998.

[10] Boskovic, D. Jovan, S. Li and R. K. Mehra, "Robust adaptive variable structure control of spacecraft under control input saturation,"*Journal of Guidance, Control, and Dynamics*, vol. 24, no. 1, pp. 14-22, 2001.

[11] Q. Hu, B. Xiao, D. Wang and E. K. Poh, "Attitude control of spacecraft with actuator uncertainty,"*Journal of Guidance, Control, and Dynamics*, vol. 36, no. 6, pp. 1771-1776, 2013.

[12] W. Luo, Y. Chu, and K. Ling, "Inverse optimal adaptive control for attitude tracking of spacecraft,"*IEEE Transactions on Automatic Control*, vol. 50, no. 11, pp. 1639-1654, 2005.

[13] F. Bayat, "Model Predictive Sliding Control for Finite-Time Three-Axis Spacecraft Attitude Tracking,"*IEEE Transactions on Industrial Electronics*, vol. 66, no. 10, pp. 7986-7996, 2019.

[14] Y. Xia, J. Zhang, K. Lu, and N. Zhou, "Finite-time tracking control of rigid spacecraft under actuator saturations and faults,"*IEEE Transactions on Automation Science and Engineering*, vol. 13, no. 1, pp. 368-381, 2016.

[15] S. Tatikonda, and S. Mitter, "Control Under Communication Constraints,"*IEEE Transactions on Automatic Control*, vol. 49, no. 7, pp. 1056-1068, 2004.

[16] J. Zhou, C. Wen and G. Yang, "Adaptive backsteppting stabilization of nonlinear uncertain systems with quantized input signal,"*IEEE transactions on Automatic Control*, vol. 59, no. 2, pp. 460-464, 2014.

[17] P. Tabuada, "Event-triggered real-time scheduling of stabilizing control tasks,"*IEEE transactions on Automatic Control*, vol. 52, no. 9, pp. 1680-1685, 2007.

[18] J. Lunze and D. Lehmann, "A state-feedback approach to event-based control,"*Automatica*, vol. 46, no. 1, pp. 211-215, 2010.

[19] B. Wu, "Spacecraft attitude control with input quantization,"*Journal of Guidance, Control, and Dynamics*, vol. 39, no. 1, pp. 176-181, 2015.

[20] B. Wu and X. Cao, "Roubust Attitude Tracking Control for Spacecraft with Quantized Torques,"*IEEE transactions on Aerospace and Electronic Systems*, vol. 54, no. 2, pp. 1020-1028, 2018.

[21] H. Sun, L. Hou, G. Zong and X Yu, "Fixed-time attitude tracking control for spacecraft with input quantization,"*IEEE transactions on Aerospace and Electronic systems*, vol. 55, no. 1, pp. 124-134, 2019.

[22] B. Wu, Q. Shen and X. Cao, "Event-triggered attitude control of spacecraft,"*Advances in Space Research*, vol. 61, no. 3, pp. 927-934, 2018.

[23] C. Zhang, J. Wang, D. Zhang and X. Shao, "Learning Observer based and event-triggered control to spacecraft against actuator faults,"*Aerospace Science and Technology*, vol. 78, no. 7, pp. 522-530, 2018.

[24] W. Liu, Y. Geng, B. Wu and D. Wang, "Neural-Network-Based Adaptive Event-triggered Control for Spacecraft Attitude Tracking,"*IEEE Transactions on Neural Networks and Learning Systems*, vol. 31, no. 10, pp. 4015-4024, 2020.

[25] H. Xie, B. Wu and W. Liu, "Adaptive Neural Network Model-based Event-triggered Attitude Tracking Control for Spacecraft,"*International Journal of Control, Automation and Systems*, vol. 1, no. 19, pp. 1-14, 2021.

[26] A. Girard, "Dynamic Triggering Mechanisms for Event-Triggered Control,"*IEEE Transactions on Automatic Control*, vol. 60, no. 7, pp. 1992-1997, July. 2015.

[27] J. Berneburg and C. Nowzari, "Robust Dynamic Event-Triggered Coordination With a Designable Minimum Interevent Time,"*IEEE Transactions on Automatic Control*, vol. 66, no. 8, pp. 3417-3428, Aug. 2021.

[28] X. Shi, Z. Lin, R. Zheng and X. Wang, "Distributed dynamic event-triggered algorithm with positive minimum inter-event time for convex optimisation problem,"*International Journal of Control*, 2020.

[29] H. Jiang, Q. Li, Y. Jiang, G. Shen, R. Sinnott, C. Tian, M. Xu, "When machine learning meets congestion control: A survey and comparison,"*Computer Networks*, vol. 192, no. 108033, 2021.

[30] R. Marx, J. Herbots, W. Lamotte, P. Quax, "Same standards, different decisions: A study of QUIC and HTTP/3 implementation diversity,"*Proceedings of the Workshop on the Evolution, Performance, and Interoperability of QUIC. 2020*, pp. 14-20, 2020.

[31] D. Scholz, B. Jaeger, L. Schwaighofer, D. Raumer, F. Geyer and G. Carle, "Towards a Deeper Understanding of TCP BBR Congestion Control,"*2018 IFIP Networking Conference (IFIP Networking) and Workshops*, pp. 1-9, 2018.

[32] Y. Bai, Y. Jing, "Event-triggered network congestion control of TCP/AWM systems,"*Neural Computing and Applications*, vol. 33, pp. 15877-15886, 2021.

[33] B. Jiang, J. Lu, Y. Liu and J. Cao, "Periodic Event-Triggered Adaptive Control for Attitude Stabilization Under Input Saturation, "*IEEE Transactions on Circuits and Systems I: Regular Papers*, vol. 67, no. 1, pp. 249-258, 2020.

[34] C. Wang, L. Guo, C. Wen, Q. Hu and J. Qiao, "Event-triggered adaptive attitude tracking control for spacecraft with unknown actuator faults,"*IEEE Transactions on Industrial Electronics*, vol. 67, no.3, pp. 2241-2250, 2019.

[35] W. Liu, Y. Geng, B. Wu and J. D. Biggs, "Distributed Constrained Control Allocation for Cellularized Spacecraft Attitude Control System,"*Journal of Guidance, Control, and Dynamics*, pp. 1-9, Oct 2021.

[36] S. Ge, C. Yang, and T. Lee, "Adaptive predictive control using neural network for a class of pure-feedback systems in discrete time,"*IEEE Transactions on Neural Networks*, vol. 19, no. 9, pp. 1599C1614, Sep. 2008.

[37] Y. Li and G. Yang, "Model-based adaptive event-triggered control of strict-feedback nonlinear systems,"*IEEE transactions on neural networks and learning systems*, vol. 29, no. 4, pp. 1033-1045, 2018.

[38] R. D. Robinett, G. G. Parker, H. Schaub, and J. L. Junkins, "Lyapunov optimal saturated control for nonlinear systems,"*Journal of Guidance, Control, and Dynamics*, vol. 20, no. 6, pp. 1083-1088, 1997.

[39] B. Chen, X. Liu, K. Liu, and C. Lin, "Direct adaptive fuzzy control of nonlinear strict-feedback systems,"*Automatica*, vol. 45, no. 6, pp. 1530-1535, 2009.

[40] L. Xing, J. Zhang, C. Liu, and X. Zhang,"Fuzzy-logic-based adaptive event-triggered sliding mode control for spacecraft attitude tracking,"*Aerospace Science and Technology*, 2021.

[41] C. Chen, C. Wen, K. Xie, Y. Zhang, and C. Chen, "Adaptive asymptotic control of multivariable systems based on a one-parameter estimation approach,"*Automatica*, vol. 83, pp. 124-132, Sep. 2017.

[42] "Sigmoid function," Wikipedia: The Free Encyclopedia. 15 Sep. 2010, [Online]. Available: https://en.wikipedia.org/wiki/Sigmoid_function

[43] K. Ning, B. Wu, C. Xu,"Event-triggered adaptive fuzzy attitude takeover control of spacecraft,"*Advances in Space Research*, vol.67, no.6, pp.1761-1772, 2021.

Hongyi Xie received the B.Eng. and M.Eng. degrees in aerospace engineering from the Harbin Institute of Technology, Harbin, China, in 2018 and 2020, respectively. Now he is pursuing the degree of Ph.D. with the Dipartimento di Ingenieria Aerospaziale at Politecnico di Milano. His research interests are spacecraft attitude and orbit control and dynamics.

Baolin Wu received the B.Eng. and M.Eng. degrees in spacecraft design from the Harbin Institute of Technology, Harbin, China, in 2003 and 2005, respectively, and the Ph.D. degree in spacecraft formation control from Nanyang Technological University, Singapore, in 2011. From 2011 to 2013, he spent two years in the satellite research and development industry in ST Electronics (Satellite Systems) Pte Ltd., Singapore. He developed algorithms for satellite attitude determination and control system. Since 2014, he has been an Associate Professor with the Research Center of Satellite Technology, Harbin Institute of Technology. Since 2020, he has been a Full Professor with the Research Center of Satellite Technology, Harbin Institute of Technology. His current research area is in spacecraft attitude control, attitude synchronization, spacecraft formation control, and trajectory optimization.

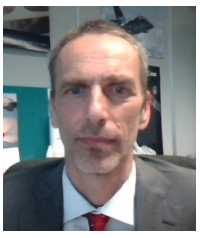

Franco Bernelli-Zazzera is currently a full professor at Politecnico di Milano where he teaches and performs research in the fields of space flight mechanics and aerospace control systems. He obtained his PhD in aerospace engineering in 1990 for his dissertation on modeling and active control of aerospace dynamic systems.

His research interests and past works include trajectory optimization for missions with low thrust propulsion and gravity assist maneuvers; trajectory optimization through a direct method for a mission to NEOs, using low-thrust propulsion both for deep space navigation and for Earth escape phase; as well as the optimization of low-thrust space trajectories. Furthermore, he has worked on the analysis and design of low-energy interplanetary transfers exploiting the invariant manifolds of the restricted three-body problem. His scientific activity also includes work on the development of a mobile rover equipped with a pure optical navigation system as well as the development of the university satellite PALAMEDE.

Dr. Bernelli Zazzera has authored or co-authored over 270 publications. He is now the President of CEAS (Council of European Aerospace Societies).